

AD 649685

**INVESTIGATION OF ELECTRONIC FRINGE DETECTOR
FOR A STELLAR INTERFEROMETER**

John Boardman and Paul Kellen

**Technical Operations, Incorporated
Burlington, Massachusetts**

Contract No. AF 19(628)-5145

Project No. 8663

FINAL REPORT

7 April 1966 through 7 February 1967

7 February 1967

**This research was sponsored by the Advanced Research Projects
Agency, ARPA Order No. 450, Amendment 2, 4**

Contract Monitor: George A. Vanasse

Distribution of this document is unlimited

Prepared for

**AIR FORCE CAMBRIDGE RESEARCH LABORATORIES
OFFICE OF AEROSPACE RESEARCH
UNITED STATES AIR FORCE
BEDFORD, MASSACHUSETTS 01720**

**DDC
APR 10 1967
A**

ARCHIVE COPY.

AFCRL-67-0117

**INVESTIGATION OF ELECTRONIC FRINGE DETECTOR
FOR A STELLAR INTERFEROMETER**

John Boardman and Paul Kellen

**Technical Operations, Incorporated
Burlington, Massachusetts**

Contract No. AF 19(628)-5145

Project No. 8663

FINAL REPORT

7 April 1966 through 7 February 1967

7 February 1967

**This research was sponsored by the Advanced Research Projects
Agency, ARPA Order No. 450, Amendment 2, 4**

Contract Monitor: George A. Vanasse

Distribution of this document is unlimited

Prepared for

**AIR FORCE CAMBRIDGE RESEARCH LABORATORIES
OFFICE OF AEROSPACE RESEARCH
UNITED STATES AIR FORCE
BEDFORD, MASSACHUSETTS 01730**

ABSTRACT

A fringe detector was constructed to detect fringes from a Michelson stellar interferometer and to relate these measurements to the characteristics of the source of illumination. A rotating reflector, a single slit, and a phototube were combined to transform the spatially-varying intensity pattern of the fringe field into a time-varying voltage signal displayed on an oscilloscope face. The oscilloscope trace was photographed and analyzed to determine fringe contrast.

The maximum sensitivity of the detector was determined to be equivalent to a source providing 10^{-10} v/cm² at a fringe contrast of 1 and a signal-to-noise ratio of 1. Modifications can provide a factor of 500 to 1000 improvement in detector sensitivity. The interferometer was determined to have potentially better resolution than a single-mirror telescope because it can electrically filter the effects of ambient background illumination and turbulence. The use of an interferometer to measure the angular size of a pie-shaped source was studied and found to be not particularly suited to this purpose.

The action of apodized and unapodized lens systems on the field due to an extended background and a small source was analyzed. The emphasis of the analysis was to consider such a system as linear in the mutual coherence function. The results indicate that no particular advantage in terms of contrast enhancement can be obtained by apodizing.

TABLE OF CONTENTS

| <u>Section</u> | <u>Page</u> |
|---|-------------|
| I INTRODUCTION | 1 |
| II ELECTRONIC FRINGE DETECTOR | 3 |
| BACKGROUND | 3 |
| FRINGE DETECTOR DESIGN | 6 |
| THEORETICAL AND EXPERIMENTAL ANALYSIS OF THE FRINGE DETECTOR | 8 |
| THEORETICAL RESEARCH | 8 |
| EXPERIMENTAL RESEARCH | 10 |
| SOURCES OF OUTSIDE NOISE | 13 |
| COMPARISON OF A TELESCOPE AND THE INTERFEROMETER | 14 |
| III INVESTIGATION OF PIE-SHAPED SOURCES | 16 |
| IV DAYLIGHT DISCRIMINATION | 20 |
| NONCONVENTIONAL DETECTION TECHNIQUES | 20 |
| UNAPODIZED LENS SYSTEM WITH PARTIALLY COHERENT FIELDS | 20 |
| APODIZED LENS SYSTEM WITH PARTIALLY COHERENT FIELDS | 29 |
| CONVENTIONAL DETECTION TECHNIQUES | 30 |
| PHOTOMETRY | 31 |
| DETECTION | 32 |
| Photoelectric | 32 |
| Photographic | 32 |
| Visual | 33 |
| V CONCLUSIONS AND RECOMMENDATIONS | 35 |
| FRINGE DETECTOR | 35 |
| PIE-SHAPED SOURCES | 36 |
| DAYLIGHT DISCRIMINATION | 37 |
| REFERENCES | 38 |

LIST OF ILLUSTRATIONS

| <u>Figure</u> | <u>Page</u> |
|---------------|--|
| 1 | Fizeau Interferometer 3 |
| 2 | Fringe Contrast $ \gamma_{12} $ As a Function of Slit Separation. 5 |
| 3 | Schematic Diagram of Fringe Detector 6 |
| 4 | Electronic Fringe Detector 7 |
| 5 | Fringe Contrast As a Function of Slit Separation for Several Angular Source Sizes 11 |
| 6 | Performance of the Fringe Detector 12 |
| 7 | Angular Size of Source As a Function of Fringe Contrast for $D = 0.67$ cm 13 |
| 8 | Intensity Distribution Over the Cone 16 |
| 9 | Experimental and Theoretical Results for $ \gamma_{12} ^2$ for $\varphi = 0$ deg 17 |
| 10 | Experimental and Theoretical Results for $ \gamma_{12} ^2$ for $\varphi = 90$ deg \pm 5 deg 18 |
| 11 | Experimental and Theoretical Results for $ \gamma_{12} ^2$ for $\varphi = 90$ deg 19 |
| 12 | Schematic of the Theoretical Optical System 21 |
| 13 | Variation of the Image Illumination from a Partially Coherent Field with Lens Aperture 25 |
| 14 | Optical System with an Incoherent and Coherent Source Used for Determining Point Source Visibility 27 |
| 15 | Variation of the Image Illumination from Coherent and Incoherent Sources with Lens Aperture 28 |

SECTION I

INTRODUCTION

This is the final report on Contract AF 19(628)-5145. The effort was conducted in three phases: (1) a study of electronic methods of detecting fringes from a Michelson stellar interferometer and the relation of these measurements to the characteristics of the source of illumination; (2) the characteristics of a pie-shaped figure as a source of illumination; and (3) a study of unconventional techniques for detecting illumination sources in the presence of ambient background illumination. The project objectives included: (1) the establishment of the feasibility of an electronic fringe detector; (2) the design, construction, operation, and testing of a prototype; (3) the determination of the best method for optimizing the fringe detector output; (4) the evaluation of atmospheric noise inputs; (5) the evaluation of the use of an interferometer to study pie-shaped sources; and (6) the examination of the general problems of daylight tracking with the methods of modern optical theory.

The original phase of this contract included only the electronic fringe detector study. When it became apparent that the sensitivity and accuracy of the techniques of phase one were adequate, phase two was initiated to study pie-shaped sources. After the first two phases were underway, the third phase was initiated to study the general problem of daylight tracking. The first two phases of this effort were reported in detail in Scientific Report No. 1 (AFCRL-66-767) entitled "Investigation of Electronic Fringe Detector for A Stellar Interferometer," dated 7 November 1966. This report reviews the more important results presented in Scientific Report No. 1 and presents the details of the daylight tracking study. For the details of phases one and two, the reader is referred to Scientific Report No. 1.

The specific type of Michelson stellar interferometer studied is called a Fizeau interferometer and consists of two apertures that produce a fringe pattern when illuminated by an incoherent source in the far field of that source. The fringe contrast can be directly related to the shape of the source and its distance from the detector by the van Cittert-Zernike¹ prediction of the mutual coherence function. This prediction holds only in the far field of the source.

Photographic and visual measurements of fringe contrast fail when the fringes vibrate because of image motion or atmospheric turbulence. Electronic fringe-contrast measurements are superior to visual and photographic measurements because the noise produced by fringe motion and other noise sources can be electrically filtered out of the signal. These electronic fringe-contrast measurements are accomplished by converting the intensity vs position relation of the fringe field to a voltage vs time relation through the use of a grating of the same frequency as the fringes that moves relative to the fringes. The transmission of the grating is monitored by a phototube that yields the desired voltage vs time signal.

For symmetric source distributions, the fringe contrast vanishes for particular separations of the input apertures. The usual determination of the angular source size relies on determination of the zero contrast separation by visual examination of the fringe field. With electronic detection, this zero point must be determined by extrapolation since it represents a point of zero signal level. We have demonstrated this capability and have shown that the angular source can be predicted from a single

measurement of the contrast function with an accuracy limited only by the available energy. This requires, of course, that the geometrical configuration and orientation of the source be known so that the general form of the coherence function can be predicted.

For this purpose we conducted a study of the mutual coherence function that exists in the far field of a pie-shaped incoherent source. We did this for selected axes by a computer study and verified the results experimentally by obtaining the optical Fourier transform of a pie-shaped source from which a full two-dimensional mapping of the coherence function could be deduced. The results show that high contrast levels can be expected only over small aperture separations and only along specific axes. This means that a brighter pie-shaped source will be needed to achieve the accuracy represented by the axially symmetric source studied under this program.

The electronic fringe detector operated well and its performance agreed well with the limitations predicted from energy and noise considerations. Its design necessarily involves some compromises, since an optimum device would have involved a level of effort incommensurate with the objectives of this contract. However, the operating characteristics of an improved device can be predicted from the same type of analysis that was used successfully on the experimental model.

The electronic fringe detector has several advantages over a single-mirror telescope. Fundamentally, of course, it can make size determinations beyond the diffraction limit of such a telescope. It is also less affected by atmospheric turbulence, image motion, and ambient background illumination, since these noise sources can be electrically filtered in the output of the electronic fringe detector.

The method we employed in analyzing the daylight discrimination problem was to formulate the effect of a lens system on a field described by its coherence function and then to attempt to find a spatial filter configuration that would optimize the contrast for a given set of conditions. Although the operation of such a filtered system differed from that of the conventional telescope, its ultimate limitations were the same. We concluded that none of the proposed techniques offered any real advantage over more conventional methods.

Sections II and III outline the results presented in Scientific Report No. 1 on the electronic fringe detector and the pie-shaped source analysis. Section IV presents the study performed on the daylight discrimination problem. Section V is a summary of the results and conclusions of all phases of this effort.

SECTION II

ELECTRONIC FRINGE DETECTOR

The basic aim of this phase of the program was to establish the feasibility of an electronic fringe detector that would operate in conjunction with a Michelson stellar interferometer. For convenience we shall refer to the combination of these two instruments as a fringe detector. This chapter is a condensation of the research and results of the fringe detector study presented in Scientific Report No. 1. The more important results are summarized, while details of the theoretical treatment, instrument calibration, and instrument fabrication have been omitted. In the first section, "Background," we discuss the basic theory of the interferometer, outline the functions the fringe detector must perform, and present the basic considerations in converting a fringe field into an electrical signal. Under "Fringe Detector Design" we discuss the design considerations, the design constructed, and alternate systems considered. In "Theoretical and Experimental Analysis of the Fringe Detector" we outline the study of the fringe detector and present the evaluation of its performance. "Sources of Outside Noise" treats the performance of the fringe detector under operational conditions and, finally, in "Comparison of Telescope and Interferometer" we treat the relative advantages of the interferometer.

BACKGROUND

The general theory of the Michelson stellar interferometer is given in Scientific Report No. 1. For our purposes, this interferometer will be considered to consist of two slits, or entrance apertures, that combine with an optical system to focus a set of fringes at a distance from the optical system equal to one focal length, as shown in Figure 1. Here the width of the central envelope of the fringes is inversely

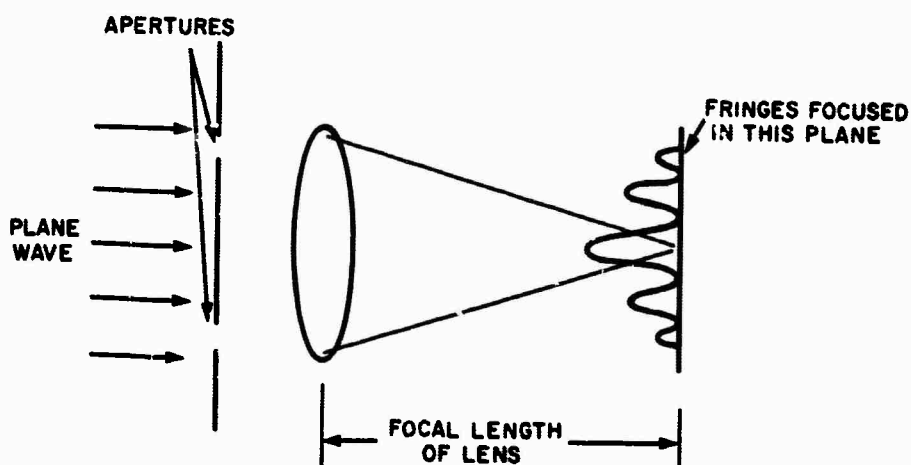


Figure 1. Fizeau Interferometer

proportional to the width of one of the slits (when the two slits are of the same width) and the width of one of the fringes is inversely proportional to the slit separation. Thus, both the spatial fringe frequency and the number of fringes in the central envelope are proportional to the aperture separation. As the aperture separation increases for a circular source, the contrast of the fringes decreases until the contrast reaches zero, as shown in Figure 2. For this source, this separation, called "extinction separation," is a measure of the angular size of an incoherent source in the far field of that source, where "angular size" means the simple angle the source subtends as viewed by the interferometer. For circular sources, the extinction separation varies inversely as the angular size of the source. Generally, for nonsymmetric sources, a well-defined extinction separation does not exist. The positions and magnitude of maximum and minimum fringe contrast, however, vary as the source is rotated. Thus, the object of this program reduces to studying electronically the inflections in the fringe pattern as a function of aperture separation and orientation.

The fringe detector must perform two functions to determine the angular size of a source: (1) It must provide for measurements made at different slit separations and (2) it must demodulate the fringe field to yield a measure of fringe contrast. This is obtained by measuring the values of the envelopes of the peaks, I_{\max} , and the valleys, I_{\min} , of the intensities of the fringe field at an arbitrary point in the field:

$$FC = \frac{I_{\max} - I_{\min}}{I_{\max} + I_{\min}}$$

For our purposes, $I_{\max} - I_{\min}$ will be considered to be the strength of an ac signal riding on top of a dc signal given by $I_{\max} + I_{\min}$.

Several techniques were investigated to detect and measure fringe contrast: nonlinear surface detectors, measurement of intensity levels at a single value of I_{\max} and a neighboring value of I_{\min} , and conversion of the field by a spatial filter. The first two were rejected because they were less sensitive and less efficient than the third, which yields a continuous signal. For a continuous signal it is possible to filter out the noise from atmospheric sources, resulting in much better sensitivity. For these reasons this method was chosen. In this context several types of gratings including cosine, square wave, and moire fringe gratings were studied. The single slit was studied as a special case of the square wave grating.

In demodulating the fringe field with a grating, we placed the grating in the plane of the fringes and moved the grating and the fringes relative to each other in a direction perpendicular to the fringes in the plane of the fringes. This yielded a time-varying transmission of the grating, which is a function of the peak-to-peak intensity difference of the fringes, $I_{\max} - I_{\min}$. A measure of $I_{\max} + I_{\min}$ can be found by chopping the signal. The transmission of the grating was then monitored by a photomultiplier tube whose output could be studied by conventional techniques.

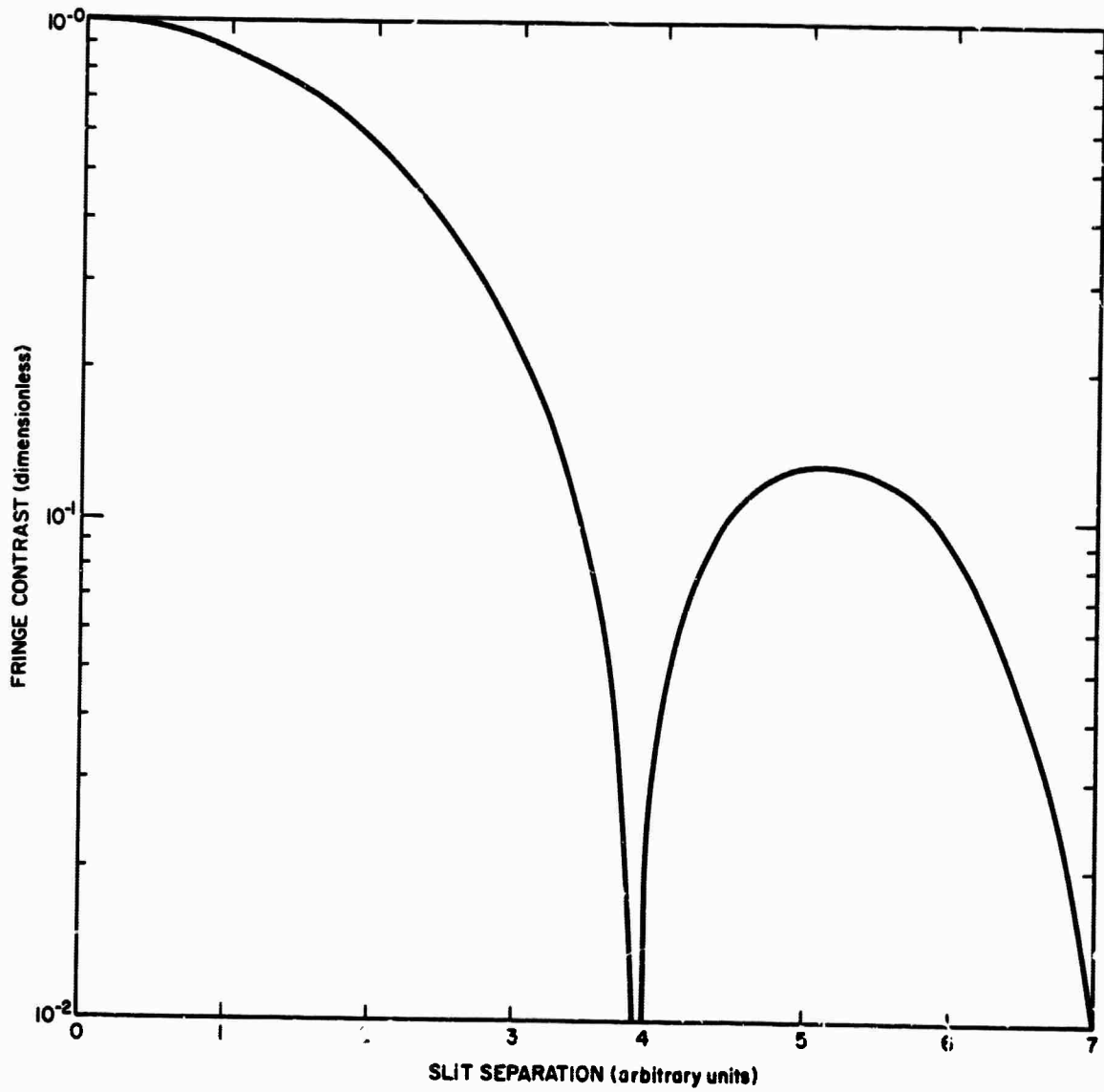


Figure 2. Fringe Contrast $|\gamma_{12}|$ As a Function of Slit Separation

FRINGE DETECTOR DESIGN

For a fixed-focal-length system, a Fizeau interferometer generates a spatial fringe frequency that varies as the slit separation. To obtain a constant fringe frequency, the possibility of using a "zoom" lens system that changes focal length by a factor of 10 was considered but discarded because of the difficulty in designing an appropriate system without either pincushion or barrel distortion. Other optical combinations to retain a constant fringe frequency would involve large changes in the optical path length. Thus, it became necessary to work with a fringe field with changing spatial fringe frequency. This led to the use of a single slit instead of a grating in front of the phototube to demodulate the field and to the use of a rotating reflector to provide linear fringe motion and chopping. The variable-separation apertures were designed to maintain the aperture height at a constant percentage of the aperture separation. This facilitated calibration by keeping the energy per fringe constant and maintaining constant degradation of the fringe contrast due to the finite height of the slits.

The arrangement of the components of the electronic fringe detector is shown schematically in Figure 3. The components are mounted on a flat aluminum plate that serves as the bottom of a light-tight box. Light enters the system only through the entrance apertures, passes through the lenses, and is reflected from one face of the rotating reflector onto the single slit in front of the phototube. In the plane containing the single slit, the light from the two apertures interferes and creates

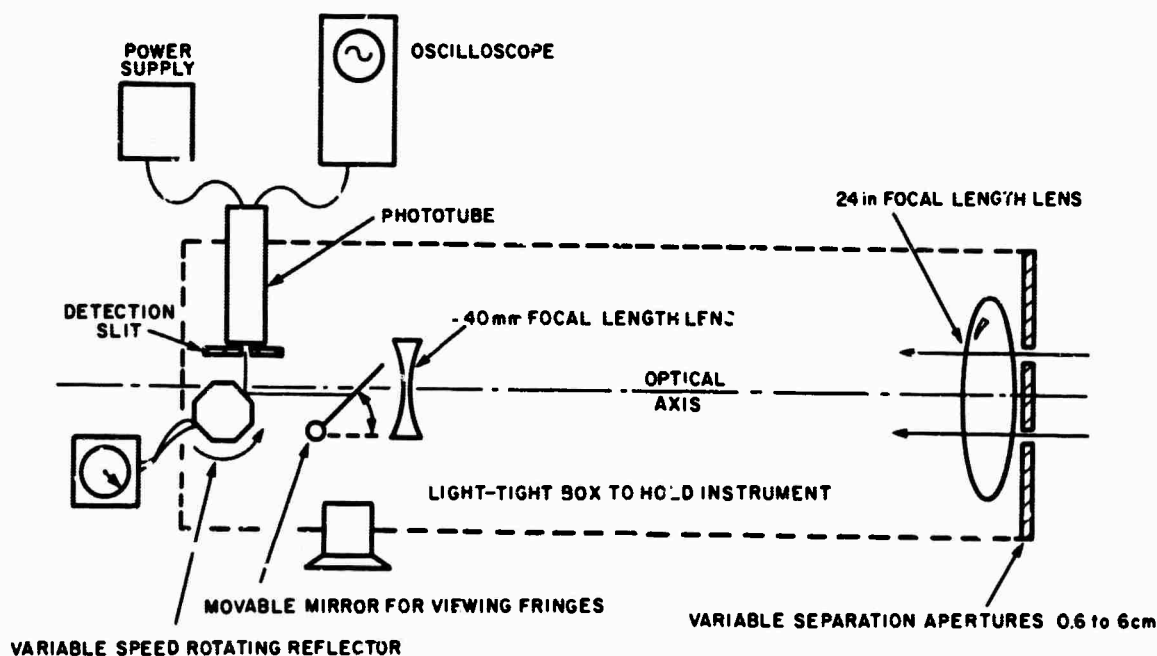


Figure 3. Schematic Diagram of Fringe Detector

spatial fringe field. If the reflector is rotating, the fringes pass by the slit and cause the light passing through the slit to vary as a function of the contrast of the fringe field. The transmission of the slit is monitored on a phototube the output from which is displayed on an oscilloscope. Here the spatial intensity distribution is observed as a voltage vs time relation. One can then determine the fringe contrast by drawing envelopes of I_{\max} and I_{\min} on the picture of the scope trace. Since the envelopes constitute a graphical average over many fringes, the accuracy of this measurement is greater than the measurement of the contrast of a single fringe. Two views of the fringe detector are shown in Figure 4.

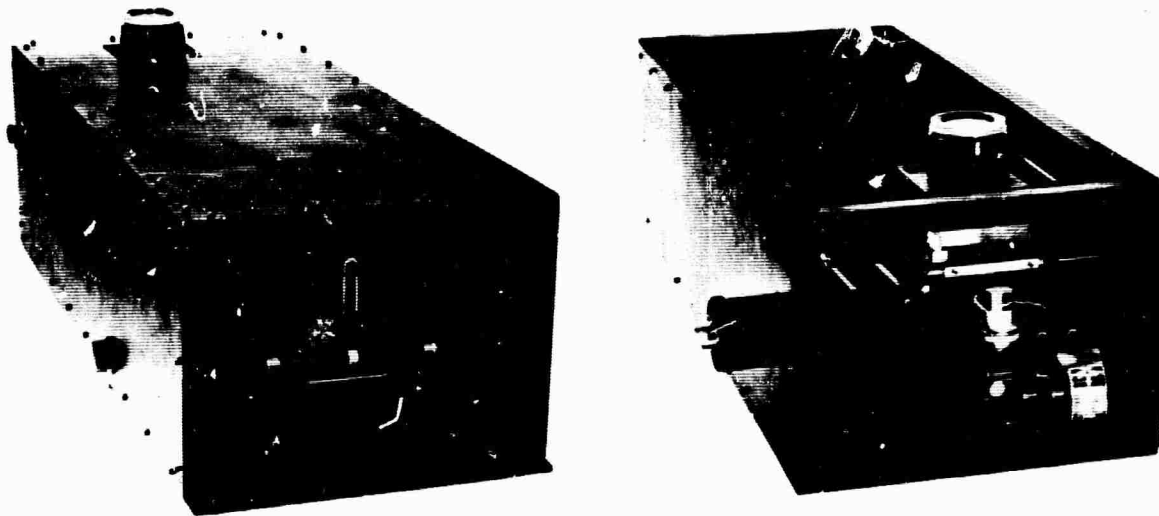


Figure 4. Electronic Fringe Detector

Several alternate system configurations were considered. While they may prove to be useful in an optimum system, they did not serve the objectives of this feasibility study. Two of the more important systems studies are presented here to indicate possible courses of development for the design of components of an ultimate fringe detector. The performance of these configurations can be directly predicted from the results of this study.

Another version of the grating-phototube combination selected is to put the single slit or grating inside the phototube. Here the focusing coil generates a magnetic field that focuses the electrons coming off the photoemissive surface onto the plane of the grating. The electric field plates then deflect the electrons so that the representation of the fringe pattern formed by the electrons is swept across the grating. The current transmitted by the grating is then amplified in the usual manner with further dynode stages. Intrinsically, this system is similar to the system in which the phototube is placed behind the grating; however, the effective area of the

photoemissive surface is equal to the area of the slit since only the "dark current" electrons from that portion of the photoemissive surface focused on the slit are amplified by the dynode chain. This has the potential advantage of a better signal-to-noise ratio than the grating-phototube combination since the signal-to-noise ratio is, in general, inversely proportional to the square root of the cathode or photoemissive surface area. All the results of this effort can be applied directly to a specialized phototube once it has been designed and the noise figures determined.

A pair of long slits parallel to a cylindrical lens is an aperture-lens combination that produces a fringe pattern containing a larger amount of energy. This results in a tall fringe pattern (same height as slits) in a direction parallel to the slits. Under these conditions, alignment of the fringe field with a grating constitutes a severe problem. Thus, such a system does not appear practical if the slit separation is to be changed. Such a system may be useful, however, if only a single measurement of fringe contrast is required. Several such systems operating in parallel could provide measurements of fringe contrast at several conditions of aperture separation. In principle, such a system can be made arbitrarily sensitive since sensitivity will increase with increasing slit length within practical limits. If a very sensitive system is required, this solution may provide the best results.

THEORETICAL AND EXPERIMENTAL ANALYSIS OF THE FRINGE DETECTOR

THEORETICAL RESEARCH

Scientific Report No. 1 treated two subjects of particular interest theoretically. The first subject was the manner in which a grating transforms the spatial intensity fluctuations of the fringe field into time-intensity fluctuations suitable for monitoring with a phototube. The second was a sensitivity analysis treating the fringe-detecting ability of the fringe detector as a whole in terms of the intensity provided by the angular source.

The conversion of the spatially distributed fringe field into a time-varying intensity can be performed by a spatial filter by moving the filter relative to the fringes in the plane of the fringes. Mathematically, this is equivalent to convolving the spatial filter with the fringe field. Since the fringe field is periodic in one dimension, the spatial filter is selected to be periodic in one dimension (i.e., grating). Letting x be position, ν_g the grating frequency in cycles per unit length, $I(x)$ the intensity of the fringe field at any point, and v the relative velocity of the fringes and the grating normalized to the grating frequency, we obtain the transmitted intensity as a function of time, $I(t)$:

$$I(t) = \int_{-L}^L I(x) (\nu_g x - vt) dx ,$$

where L is one half the length of the grating in a direction perpendicular to the fringes. The fringe field may be described in one dimension by

$$I(x) = I_0(1 + FC \cos \nu_f x) ,$$

where I_0 is the average intensity, FC is the fringe contrast with a value between 0 and 1, and ν_f is the spatial fringe frequency. In solving for $I(t)$, we obtain an expression of the form

$$I(t) = K(1 + D \cdot FC \cdot \cos vt) .$$

Here, D is the modulation index, which is a function of the grating, and K is a constant proportional to I_0 and the average transmission of the grating.

Based on such an approach, Scientific Report No. 1 considered the theory of fringe demodulation by gratings including moiré fringe, cosine, and square wave gratings. The single slit, a degenerate case of the square wave grating, was also considered. The modulation index for the single slit was found to be $\sin(\pi c \nu_f) / \pi c \nu_f$, where c is the slit opening in cm and ν_f is the fringe frequency in cycles per centimeter.

The usefulness of an electronic fringe detector is directly related to its sensitivity. Scientific Report No. 1 included a sensitivity analysis of the fringe detector to provide a better understanding of how the fringe detector could be constructed as well as to point out the techniques for analysis in such an instrument. The result of this analysis was that the energy density on the fringe detector required for the detection of fringes with a fringe contrast of 1 is

$$\text{required energy density} = \frac{ENI \sqrt{\Delta f}}{0.2 (\Delta s)^2} \times \frac{1}{D} \times \frac{1}{p} ,$$

where D is the modulation index of the single slit, p is the portion of the energy in a single fringe transmitted by the slit, ENI is the equivalent noise input of the phototube, Δs is the width of the entrance aperture, and Δf is the bandwidth of the electrical filtering process. The height of the entrance apertures was maintained at 0.1 times the aperture separation and as such does not appear in the above equation. Using the above equation, we calculated the minimum detectable signal to be $2.8 \times 10^{-10} \text{ W/cm}^2$ incident on the interferometer. The minimum detectable signal was measured to be $4 \times 10^{-10} \text{ W/cm}^2$.

EXPERIMENTAL RESEARCH

The experimental work was concentrated on three problems — noise, instrument calibration, and the performance of the fringe detector. A large portion of the experimental research concerned obtaining the proper electrical filter for an acceptable signal-to-noise ratio. The problem of electrical noise was somewhat more involved than anticipated. It has become clear that almost all the fundamental problems encountered in constructing an electronic fringe detector are ultimately noise problems and may be treated as such. This includes not only the standard sources of electrical noise, but also the effects of atmospheric turbulence, fluctuations in source brightness, vibrations in the fringe detector, background illumination, and target motion. For the majority of our measurements, however, the noise limit was set by the shot noise in the phototube.

The electrical filter that gave the best results was a 250 Hz low-pass filter. Once this electrical filter was obtained, the calibration of the instrument and the evaluation of the performance of the fringe detector proceeded without delay. For details of the filter investigations and the calibration procedures, the reader is referred to Scientific Report No. 1.

To evaluate the performance of the fringe detector, collimated light from a lens-pinhole combination was used to obtain sources with angular dimensions suitable for use with the interferometer. Lenses with focal lengths of 48 in. and 15 in. were used in various combinations with a 25 μ and a 52 μ pinhole to yield source sizes of 1.96×10^{-5} , 4.28×10^{-5} , 6.55×10^{-5} , and 1.36×10^{-4} rad. Figure 5 combines all the measurements of angular source size on a single scale for comparison. As the source size (intensity) increases, the point of fringe extinction separation becomes more clearly defined because the larger sources are brighter and, hence, the signal-to-noise ratios are better. For the 6.55×10^{-4} rad case, the data started on the second maximum of fringe contrast. The measured fringe contrast is lower than the theoretical value near the first maximum because the fringe contrast is degraded by the finite size of the entrance apertures, and the demodulation of the fringes by the detection slit is less than 1. In the region near the first maximum, noise was generally not significant. At the second maximum, the measured fringe contrast was high because of the contribution of the noise to the measured signal. The false fringe contrast measured at extinction separation is a measure of the noise level of the system.

For the measurements made, the signal-to-noise ratio can be shown to be

$$\frac{S}{N} = \frac{FC \sqrt{S_e}}{k \sqrt{\Delta f}}$$

where FC is the fringe contrast, S_e is the signal of the envelope, and k is a constant of the phototube in question. Using this formula we plotted the solid line in Figure 6 as a prediction of the noise level for each level of incident radiation in

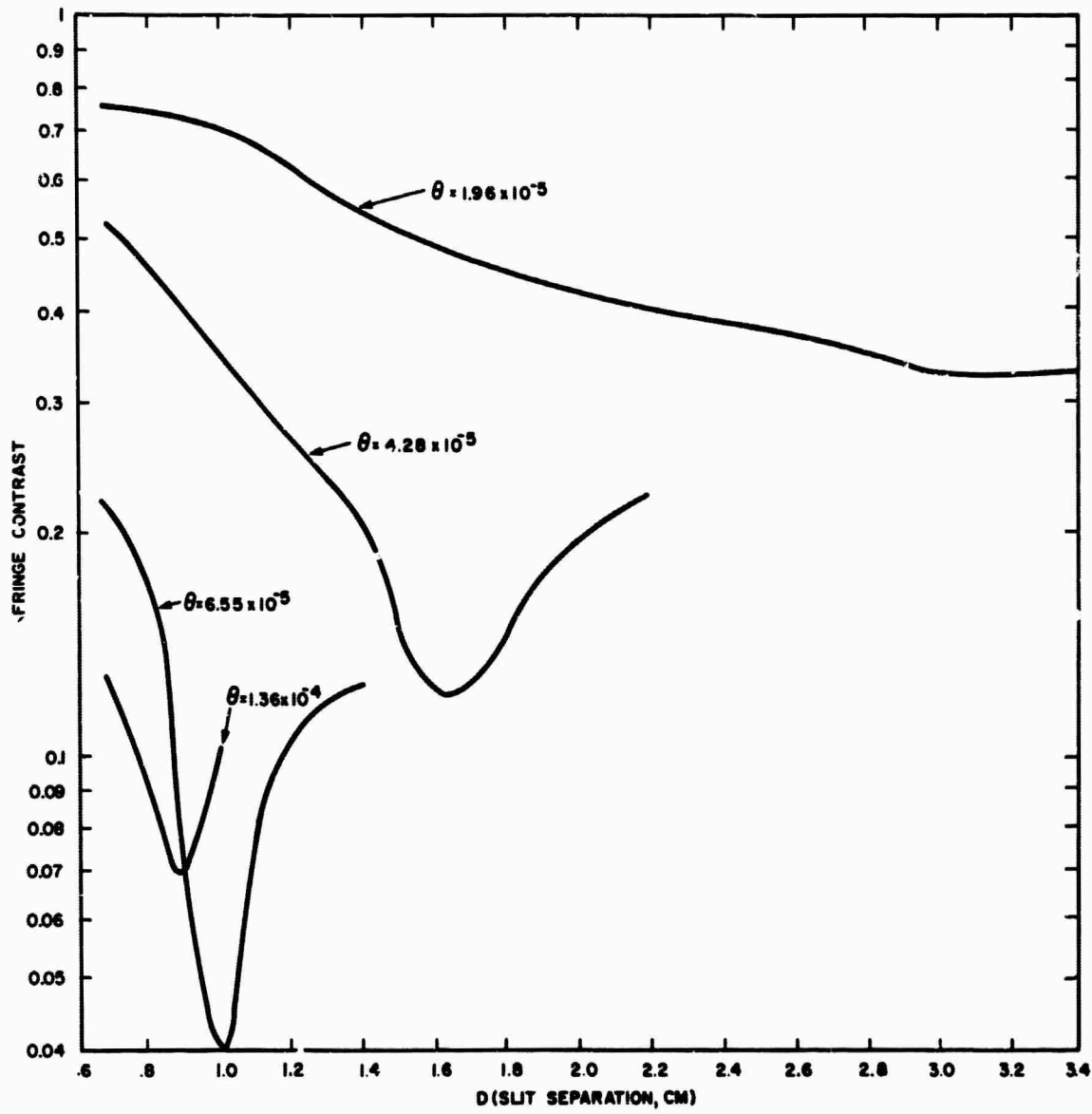


Figure 5. Fringe Contrast As a Function of Slit Separation for Several Angular Source Sizes

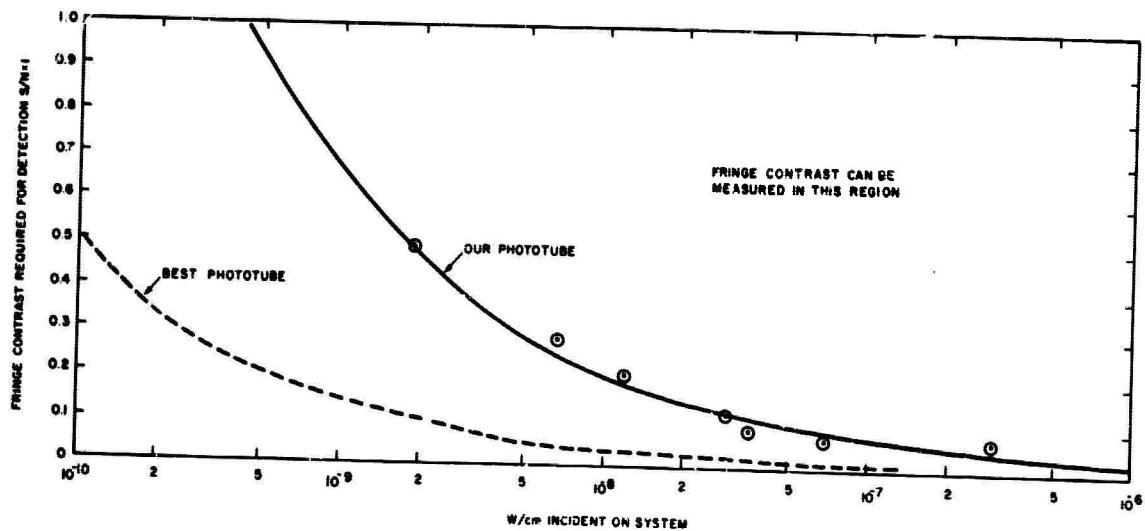


Figure 6. Performance of the Fringe Detector

watts per centimeter squared. We derived this from the known brightness of the mercury arc source as specified by the manufacturer and from the noise level at extinction separation for the 1.96×10^{-5} source. This noise level is the fringe contrast in watts per centimeter squared that can be detected at a signal-to-noise ratio of 1. Any combination of fringe contrast and watts per centimeter squared lying in the upper right-hand part of the graph can be detected with this system. The circled data points are the noise levels for various intensities measured with different-sized sources. These data points seem to be in excellent agreement with the predicted curve. To further support these data, we studied the 6.55×10^{-5} source with 0.3, 0.8, and 1.6 neutral density filters in front of it. The results here are also shown as circled points in Figure 6. The dotted line in the figure represents what can be done with the best available phototube (cooled, and so forth), which would be better than our tube by about a factor of 20.

Figure 7 shows the fringe contrasts at an entrance aperture separation of 0.67 cm measured for various-sized sources. This demonstrates that the angular source size can be predicted from a single measurement of fringe contrast. This, of course, allows the use of a fixed aperture separation and, hence, a constant spatial fringe frequency, which in turn would lead to improved sensitivity for the instrument since a grating could be used instead of a slit.

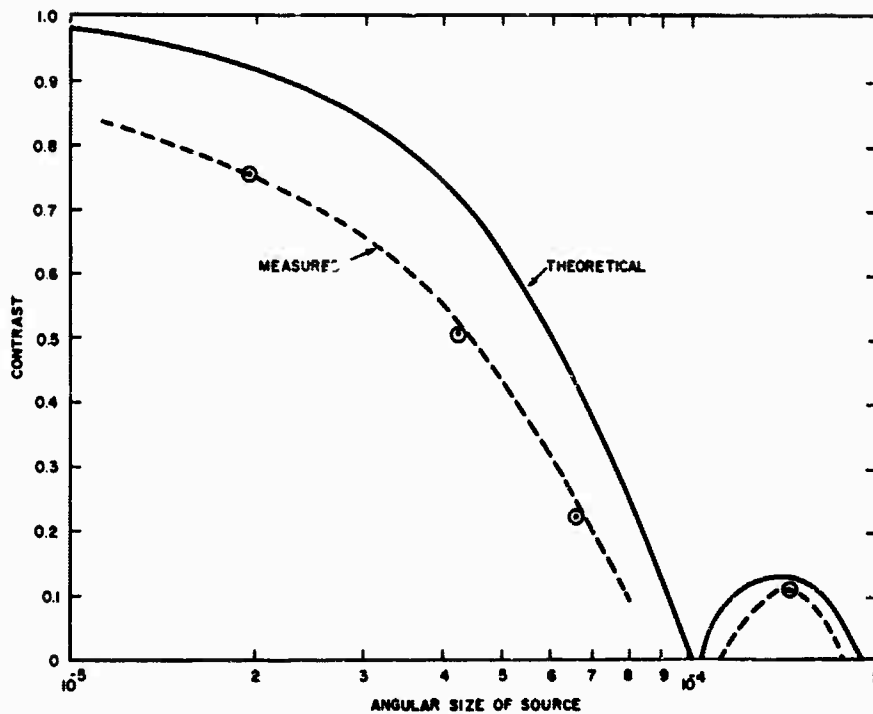


Figure 7. Angular Size of Source As a Function of Fringe Contrast for $D = 0.67$ cm

SOURCES OF OUTSIDE NOISE

The five types of outside-noise sources considered were atmospheric turbulence, vibration or movement of the detector, image motion, brightness fluctuations in the target, and background illumination.

Atmospheric turbulence, movement of the detector, and image motion are similar in that they all produce phase modulation of the ac signal coming out of the phototube. All three sources of noise cause apparent image motion, which causes the fringe field to move about on the slit. The frequency and amplitude of this unwanted fringe motion is transformed by the rotating reflector and the detection slit into a phase modulation of the signal. The bandwidth of the fringe detector with respect to these phase modulations, however, is much less than the quoted value of 250 Hz (electrical filter bandwidth) because of the manner in which the fringe contrast was measured. As previously discussed, the fringe contrast given by the oscilloscope trace is determined by locating the envelope of I_{\max} and I_{\min} and measuring the fringe contrast from this envelope rather than trying to resolve the contrast of single fringes. There is no direct way in which the phase modulation can affect the envelope of the amplitude of the ac signal, although phase modulation can affect the apparent contrast of a single fringe.

Fluctuations in brightness of the source are a nonlinear source of noise, since the signal-to-noise ratio is proportional to the square root of the source brightness. Brightness fluctuations will also create false fringes in that the dc signal output of the phototube will change with the source brightness fluctuations. It is clearly possible for source brightness fluctuations of the proper frequency to generate a fringe pattern where the fringe contrast is actually equal to zero. This production of apparent fringes may be combatted by discrimination techniques that independently monitor the brightness of the source with a second channel and electronically correct the fluctuating intensity of what should be the dc part of the signal coming from the phototube. The fluctuating signal-to-noise ratio will still be present, however, and will contribute to inaccuracies in the measurement related to those frequency components of the fluctuating signal that are within the electrical bandpass of the system.

Background illumination introduces noise in the form of an increase in the dc component of the signal and an increase in the shot noise of the phototube. The increase in the dc signal is proportional to the background illumination. The increase in the dc component can be compensated in the same manner as the fluctuating source intensity with an additional channel to monitor the background illumination. This additional channel can also compensate for fluctuating background illumination. The increase in shot noise has the apparent effect of increasing the equivalent noise input (ENI) of the phototube, thus reducing the sensitivity. Designing the fringe detector with the smallest detecting area consistent with other requirements limits the field of view of the instrument and, hence, reduces the effects of background illumination to a minimum.

COMPARISON OF A TELESCOPE AND THE INTERFEROMETER

This section reviews the known advantages of the single-mirror telescope and the Michelson stellar interferometer and defines those parameters that must be measured to establish the relative usefulness of each type of instrument, with particular attention to adverse atmospheric effects.

Although a single mirror telescope can obtain the same information as the interferometer, the interferometer has several advantages. The most obvious is in the measurement of sources with images smaller than the diffraction limit of the telescope. In this case no measurement can be made by the telescope. The interferometer has no such limit and could therefore measure the angular size and position of any incoherent source within the practical limits dictated by mechanical stability and energy losses.

In the common range of measurement, the interferometer is again advantageous when the measurement must be made through a turbulent medium such as the atmosphere because the effects of the medium on the interferometer are of a different character than those on the telescope. We can broadly divide the atmospheric effects into three categories: (1) fluctuations of the image intensity, (2) fluctuations in the image size, and (3) fluctuations in the apparent position of the image. These variations are characterized by their amplitude and frequency distribution.

Fluctuations in the intensity represent a fluctuating signal for both instruments. With the interferometer, the fluctuation represents a noise source resulting in a decrease in sensitivity. In the telescope the measurement accuracy will be maintained unless the fluctuations are either of such a magnitude or occur at such a rate as to cause operator fatigue.

Changes in apparent image size are due to distortions in the wavefront as it transverses the medium. These changes allow only a measurement of the average size. The interferometer is not susceptible to this difficulty directly but will be affected by changes in the correlations of the fields at a pair of points. It is difficult to compare the relative magnitudes of these effects since relatively little information is available on the latter problem.

Changes in the apparent image position can be caused by either the turbulent medium or improper tracking. The problem is one of relative motion, and the discussion of the effects applies for either cause. In the interferometer, this noise source can be effectively filtered. In the telescope, both the frequency and amplitude of the fluctuations will affect the degree of degradation and, since no filtering is available, no measurement can be made if the fluctuations have components faster than the resolution time of the eye.

A final effect of atmospheric transmission is the loss of contrast with range. Since the ambient level does not depend on the target range, this loss of contrast reflects a loss in signal energy. This energy is unavailable regardless of the type of instrument used.

To establish the relative usefulness of the two instruments, atmospheric-induced source motion, reduction in spatial coherence, ambient background illumination, and brightness fluctuations must be studied. For a proper comparison, tracking accuracy must also be considered.

SECTION III

INVESTIGATION OF PIE-SHAPED SOURCES

The method of measuring angular sizes of small circular sources with a Michelson stellar interferometer (by measuring the beam separation for which the fringe contrast goes to zero) is well established.¹ However, while a similar analysis may be applied to pie-shaped sources, it is considerably more complicated because of the rotational asymmetry of the source and other factors such as orientation and a nonuniform intensity distribution. Hence, this investigation was undertaken to determine the feasibility of using a Michelson stellar interferometer to study pie-shaped sources. In particular, calculations of the fringe contrast or equivalent $|\gamma_{12}|$ were made and verified experimentally.

The background mathematics, the computer program, the experimental program, and the results were discussed in detail in Scientific Report No. 1. Here we briefly summarize the theoretical and experimental treatment of the problem and present the results for the case of uniform illumination of the cone.

Theoretically, $|\gamma_{12}|$ may be calculated by application of the van-Cittert Zernike theorem. According to this theorem, if the dimensions of the source and the separation of the apertures of the Michelson stellar interferometer are small compared to the distance between the interferometer and the source, the degree of coherence $|\gamma_{12}|$ is given by the absolute value of the normalized Fourier transform of the source intensity distribution.¹ The computer calculations consisted of applying the van Cittert-Zernike theorem to a 10 deg cone. The radius of the cone was divided into three segments each of constant intensity (Figure 8). The quantities B and B' as functions of the radii r_1 , r_2 , and r_3 therefore define the nonuniform intensity distribution. The radii r_1 were fixed at $1/40 r_3$ and $39/40 r_3$, respectively. The ratio of the relative intensities B'/B was given values of 1, 10, and 100. The results were found, generally, to lack well-defined zeros in $|\gamma_{12}|$ or other characteristics that would permit the geometry of the pie-shaped source to be accurately studied with a Michelson stellar interferometer.

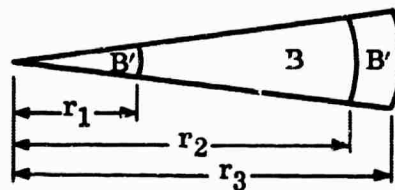


Figure 8. Intensity Distribution Over the Cone

To verify the calculated values of $|\gamma_{12}|$ for $B/B = 1$, a 10 deg cone, 0.5 mm high was illuminated coherently with laser light. This illuminated cone was Fourier-transformed by standard optical techniques and the result was recorded on film. Microdensitometer traces of the film were then combined with the calculated data. The results are shown in Figures 9, 10, and 11. In all cases ω is the angle measured from

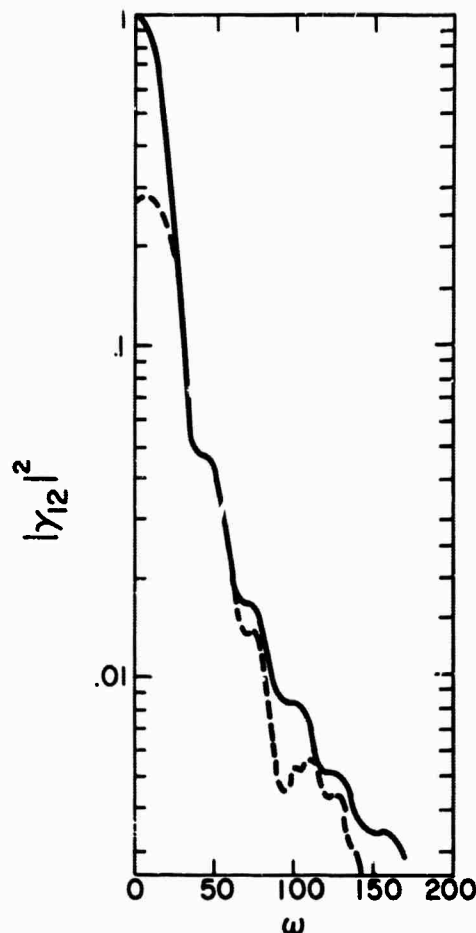


Figure 9. Experimental and Theoretical Results for $|\gamma_{12}|^2$ for $\omega = 0$ deg

the plane passing through the axis of the cone and lying along the line between the source and the interferometer. For $\omega = 0$ deg and 90 deg, there are no clearly defined maxima. For $\omega = 90$ deg \pm 5 deg, the second maxima have such a low value that it will probably be undetectable. For this application $|\gamma_{12}|^2$ should probably have a value greater than 0.001 at the second maxima since, according to Figure 6, values of $|\gamma_{12}|$ greater than $\sqrt{.001} = .032$ are detectable only for relatively intense illuminations incident on the interferometer. These unencouraging results are characteristic of the results obtained. The situation did improve somewhat for $B/B = 100$. In spite of this, the results indicate that pie-shaped sources are not particularly well suited for study by interferometry techniques.

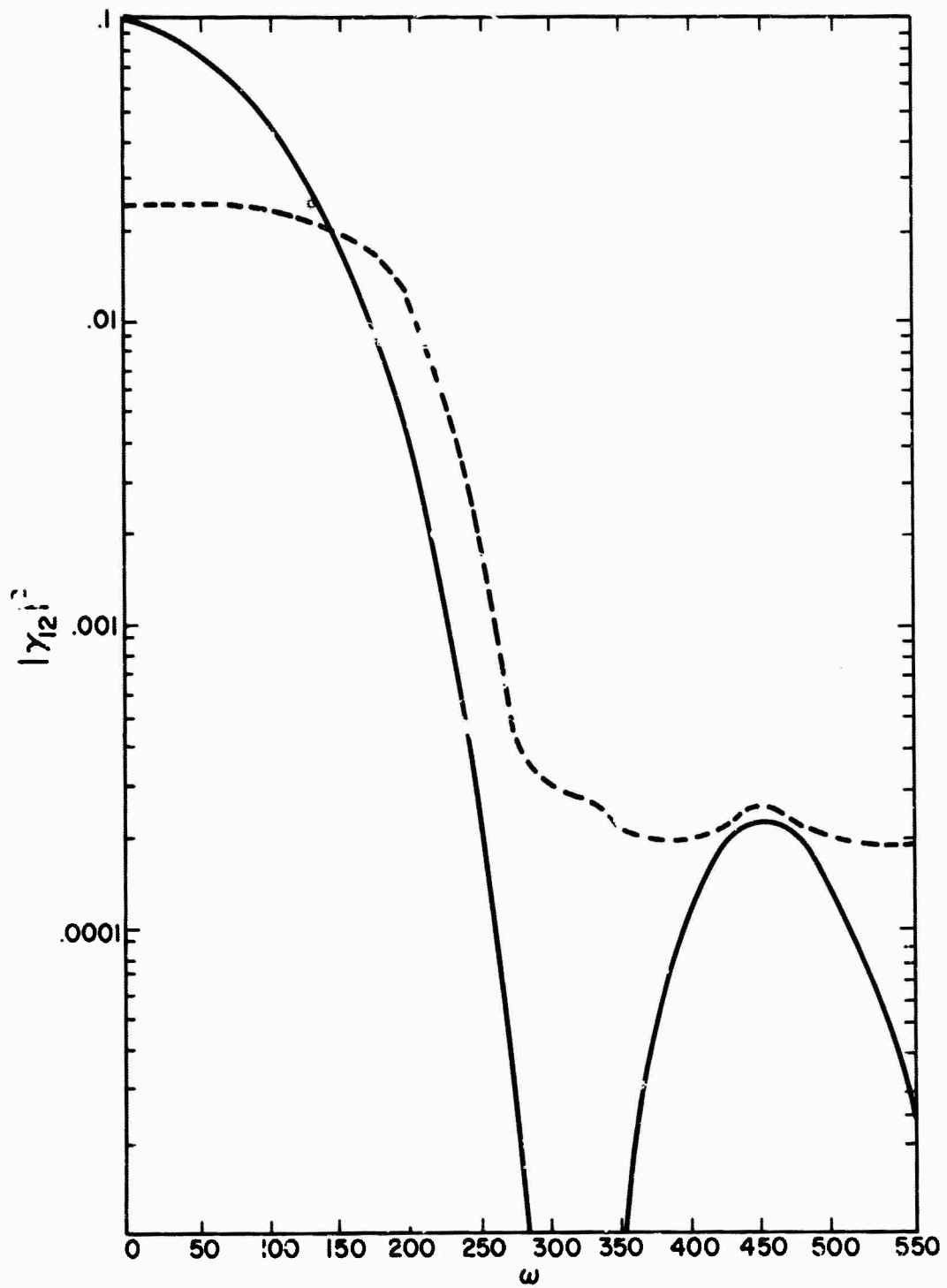


Figure 10. Experimental and Theoretical Results for $|\gamma_{12}|^2$ for $\omega = 90 \text{ deg} \pm 5 \text{ deg}$

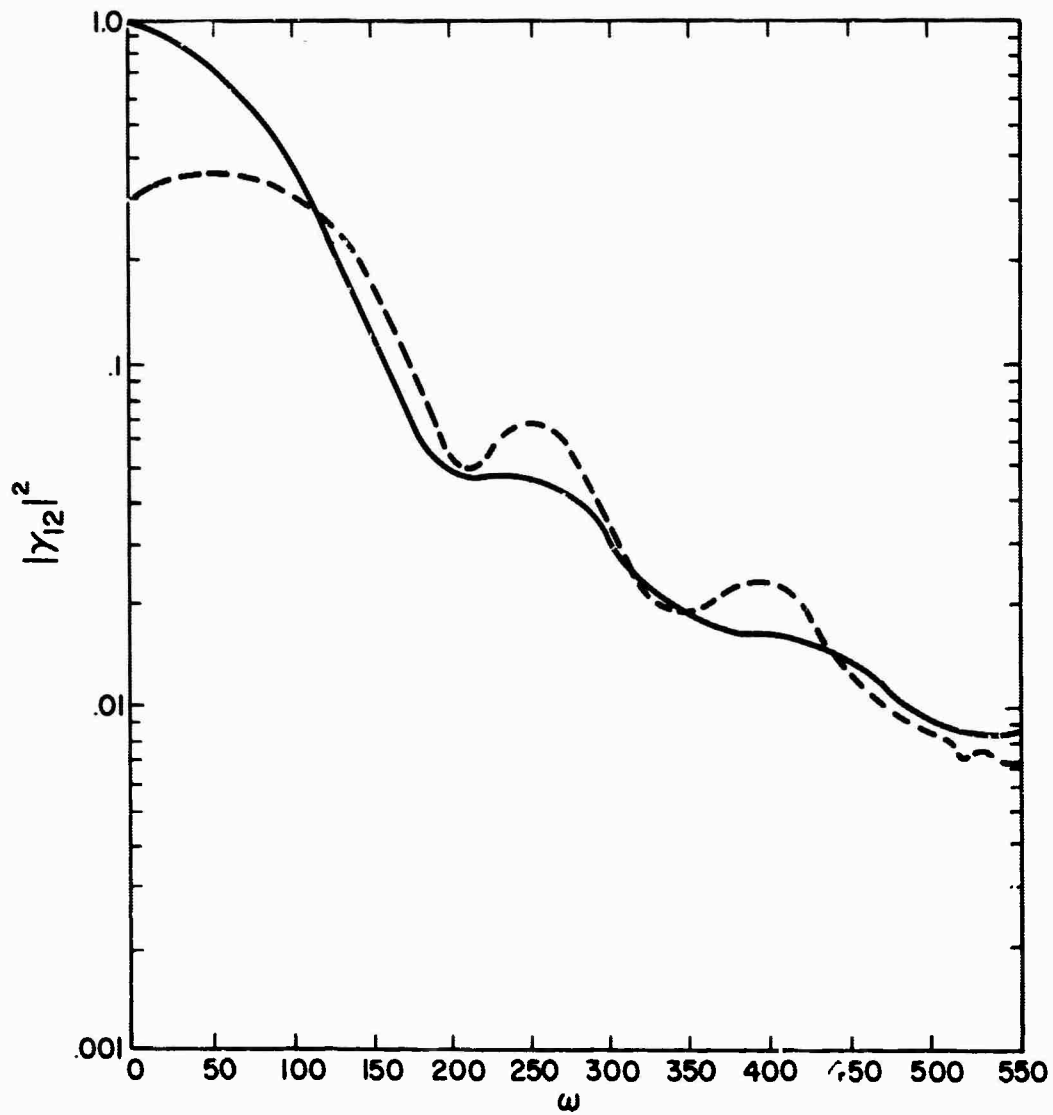


Figure 11. Experimental and Theoretical Results for $|\gamma_{12}|^2$ for $\omega = 90$ deg

SECTION IV

DAYLIGHT DISCRIMINATION

Phase three of the contract dealt with the detection of a small object against an incoherent background. The aim was to improve the detectability of this object by enhancing the contrast between the object and its background. The background illumination was assumed to have the properties of natural skylight.

Our information about either of these sources is contained in their optical field. It is the properties of this field and their relation to the source that must be examined to determine if any contrast enhancement is possible. For example, if each source were polarized in a different direction or if they radiated in different spectral regions, enhancement could be obtained by employing the proper polarizer or spectral filter.

In this investigation we were principally concerned with the coherence properties of the two fields. The coherence function of a field is, in general, a measure of the cross correlation of the field amplitude at different space and time points. By a suitable contraction of its argument it can be shown to yield the field intensity. Its significance can be grasped from a simple experiment. If a piece of photographic film were exposed in front of a lens located some distance from a luminous object, a uniform fogging would be measured. If it were exposed in the image plane we would obtain an image of the intensity distribution of the object. Thus, at the lens, the object information is not carried by the field intensity, which is uniform, but in the field amplitude.

The problem of proper use of imaging systems has been studied for many years by astronomers. Our approach differed from the conventional analysis in that we did not restrict our view of lens systems to be image-forming systems. Rather, we considered them as elements of a linear system. We also studied conventional techniques to compare results.

NONCONVENTIONAL DETECTION TECHNIQUES

UNAPODIZED LENS SYSTEM WITH PARTIALLY COHERENT FIELDS

It is well known that lenses have a qualitatively different response to coherent and incoherent aperture distributions. It has also been established that the degree of spatial coherence in the field of an incoherent source is linearly related to the angular source size. For a source such as natural skylight, the degree of coherence will be small, no greater than the degree of coherence of direct-sun illumination. Thus, the degree of coherence in the field of 4 to 100 μ rad sources is from 100 to 2500 times as great as that of skylight. One can choose the diameter of the objective such that these two fields can be considered incoherent and coherent, respectively. In these extreme cases the operation of an unapodized lens is well known. For the incoherent case an "image" will be produced. Since the sky is essentially a uniform radiator, the image will simply be a uniform illumination of the image plane. For the coherent case an Airy pattern is produced. This pattern is characteristic of the lens and has the form

$$I(\rho, \theta) = I_0 \left[\frac{2 J_1(k\rho R)}{k\rho R} \right]^2,$$

where $k = 2\pi/\text{wavelength}$, R is the radius of the lens, ρ and θ are the coordinates of the image plane, and $J_1(x)$ is the first-order Bessel function. The total energy in either the coherent or incoherent pattern will be proportional to the lens area. However, the area under the central lobe of the function $J_1(x)$, which contains 85% of the energy of the pattern, will decrease as R^2 or in proportion to the aperture, so that for changing aperture A the respective intensities vary as

$$\frac{I_{\text{coherent}}}{I_{\text{incoherent}}} = c \frac{A^2}{A} = c A \quad .$$

This is the known result that to see a star or small object in the daytime you must open the aperture. This result holds only as long as the field of the small object remains coherent over the lens aperture.

The degree of coherence is a measure of the ability of the fields from two spatially separated points to superpose coherently. This can be measured by examining the contrast of fringes produced by interfering the light from these two points. The coherence interval (CI) is that separation for which the contrast becomes zero. For a circular source it is

$$CI = \frac{1.22 \lambda}{\alpha} \quad ,$$

where α is the angular size of the source and λ is its wavelength. The coherence interval for the range of angular source size being considered is 0.5 cm to 50.0 cm. Thompson, Shore, and Whitney² have examined the patterns produced by a partially coherent field on a lens as a function of the ratio of the coherence interval/lens diameter. From their results it is seen that for even a moderate telescope aperture we are departing from the region of validity of the previous calculation.

To properly evaluate the case of the clear aperture we must calculate image distribution under more general conditions. For Figure 12, we shall calculate the

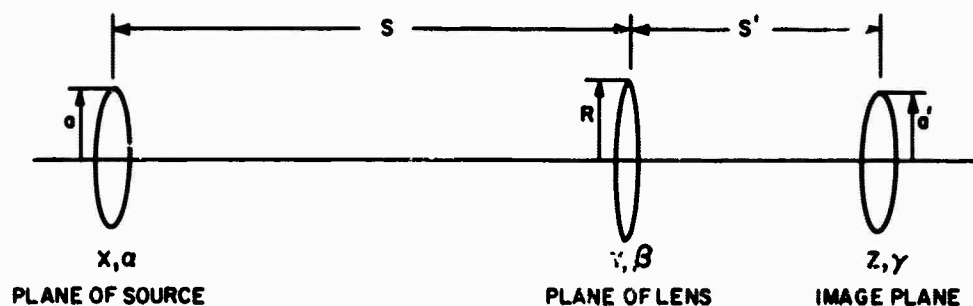


Figure 12. Schematic of the Theoretical Optical System

propagation of the mutual coherence function from a small incoherent source of radius a to the image plane of a lens of radius R and obtain the total energy in a small area, radius a' , in the center of the image. The integrated intensity over a' can be written

$$I_0 \int \delta(\bar{x}_1 - \bar{x}_2) e^{\frac{ik}{2s} \left[x_1^2 + y_1^2 - 2x_1 y_1 \cos(\alpha_1 - \beta_1) - x_2^2 - y_2^2 + 2x_2 y_2 \cos(\alpha_2 - \beta_2) \right] - \frac{ik}{2f} (y_1^2 - y_2^2)} \times e^{\frac{ik}{2s'} \left[y_1^2 + z_1^2 - 2y_1 z_1 \cos \beta_1 - \gamma - y_2^2 - z^2 + 2y_2 z \cos(\beta_2 - \gamma) \right]} \quad (1)$$

$$x_1 dx_1 d\alpha_1 x_2 dx_2 d\alpha_2 \\ y_1 dy_1 d\beta_1 y_2 dy_2 d\beta_2 \\ z dz d\gamma \quad .$$

Using the imaging condition $1/s + 1/s' = 1/f$, one sees that the quadratic terms in y_1 and y_2 cancel identically. Expression (1) simplifies to

$$I_0 \int e^{ik \left[-\frac{xy_1}{s} \cos(\alpha - \beta_1) + \frac{xy_2}{s} \cos(\alpha - \beta_2) - \frac{y_1 z}{s'} \cos(\beta_1 - \gamma) + \frac{y_2 z}{s'} \cos(\beta_2 - \gamma) \right]} \quad (2)$$

$$x dx d\alpha z dz d\gamma \\ y_1 dy_1 d\beta_1 y_2 dy_2 d\beta_2 \quad .$$

Consider the first and third terms in the exponent:

$$-\frac{xy_1}{s} \cos(\alpha - \beta_1) - \frac{zy_1}{s'} \cos(\beta_1 - \gamma) = -\left(\frac{xy_1}{s} \cos \alpha + \frac{zy_1}{s'} \cos \gamma \cos \beta_1 \right) \\ \left(-\frac{xy_1}{s} \sin \alpha + \frac{zy_1}{s'} \sin \gamma \sin \beta_1 \right) \quad (3)$$

Define P and ϕ by:

$$P^2 = \frac{x^2}{s^2} + \frac{z^2}{s'^2} + \frac{2xz}{ss'} \cos(\alpha - \gamma) = \left| \frac{\vec{x}}{s} + \frac{\vec{z}}{s'} \right|^2 \quad (4a)$$

$$P \cos \phi = \frac{x}{s} \cos \alpha + \frac{z}{s'} \cos \gamma \quad (4b)$$

Using (4a) and (4b) in Expression (2), one obtains

$$\begin{aligned} &= I_0 \int e^{ik[-y_1 P \cos(\phi - \beta_1) + y_2 P \cos(\phi - \beta_2)]} y dy_1 d\beta_1 y_2 dy_2 d\beta_2 x dx d\alpha dz d\gamma \\ &\sim I_0 \int \left[J_0(kyP) y dy \right]^2 x dx d\alpha dz d\gamma \quad (5) \\ &\sim I_0 R^2 \int \left[\frac{J_1(kRP)}{kP} \right]^2 x dx d\alpha dz d\gamma \\ &= I_0 R^2 \int \left[\frac{J_1\left(k\rho \left| \frac{\vec{x}}{s} + \frac{\vec{z}}{s'} \right| \right)}{k \left| \frac{\vec{x}}{s} + \frac{\vec{z}}{s'} \right|} \right]^2 d\vec{x} d\vec{z} \end{aligned}$$

This remaining integral does not readily lend itself to evaluation except when $a' \ll 1$, i. e., the detection area is very small. In this case the integral is essentially constant for the \vec{z} integral and the expression reduces to

$$I_0 k^2 2\pi^2 a'^2 \int_0^a \left[\frac{J_1\left(kR \left| \frac{\vec{x}}{s} \right| \right)}{k \left| \frac{\vec{x}}{s} \right|} \right]^2 x dx \quad (6)$$

From inspection of the integral one may use the approximation

$$\int_0^y \left[\frac{J_1(z)}{z} \right]^2 dz \approx A (1 - e^{-By}) \quad (7)$$

Expression (6) may be integrated by parts:

$$\begin{aligned}
 & R^2 \int_0^{\frac{kR}{s}} \left[\frac{J_1(z)}{z} \right]^2 z \, dz \\
 &= k^2 z (1 - e^{-Bz}) \Big|_{z=0}^{z=\frac{kRa}{s}} - R^2 \int_0^{\frac{kR}{s}} (1 - e^{-Bz}) \, dz \quad (8) \\
 &= -\frac{kaR^3}{s} e^{-B\frac{kaR}{s}} + \frac{R^2}{B} (1 - e^{-B\frac{kaR}{s}})
 \end{aligned}$$

From this expression we may immediately recover the incoherent and coherent limits. We note that s/ka is proportional to the coherence interval previously mentioned and that the proportionality constant is nearly one. Therefore, kaR/s is roughly the ratio of the coherence interval to the lens diameter. In case i (coherent or $kaR/s \ll 1$), Expression (8) becomes

$$\approx \left(\frac{k^2 a^2}{2s^2} \right) R^4 .$$

In case ii (incoherent or $kaR/s \gg 1$), we have

$$\approx \frac{R^2}{B} .$$

We may examine the limits of these regions more precisely: $kaR/s \gg 1$ will hold when

$$e^{-B\frac{kaR}{s}} = e^{-x} < 0.1$$

and

$$xe^{-x} < 0.1$$

The stronger condition is the second one, and this gives $x > 3.7$ or that the ratio of coherence interval to lens diameter is about 1:7. For $kaR/s \ll 1$, the limit will be near

$$e^{-x} > 0.9 ,$$

which gives a ratio of coherence interval to lens diameter of 3:1. The value of Expression (8) in the intermediate region was calculated and a plot of central energy density vs the ratio of coherence interval to lens diameter is shown in Figure 13.

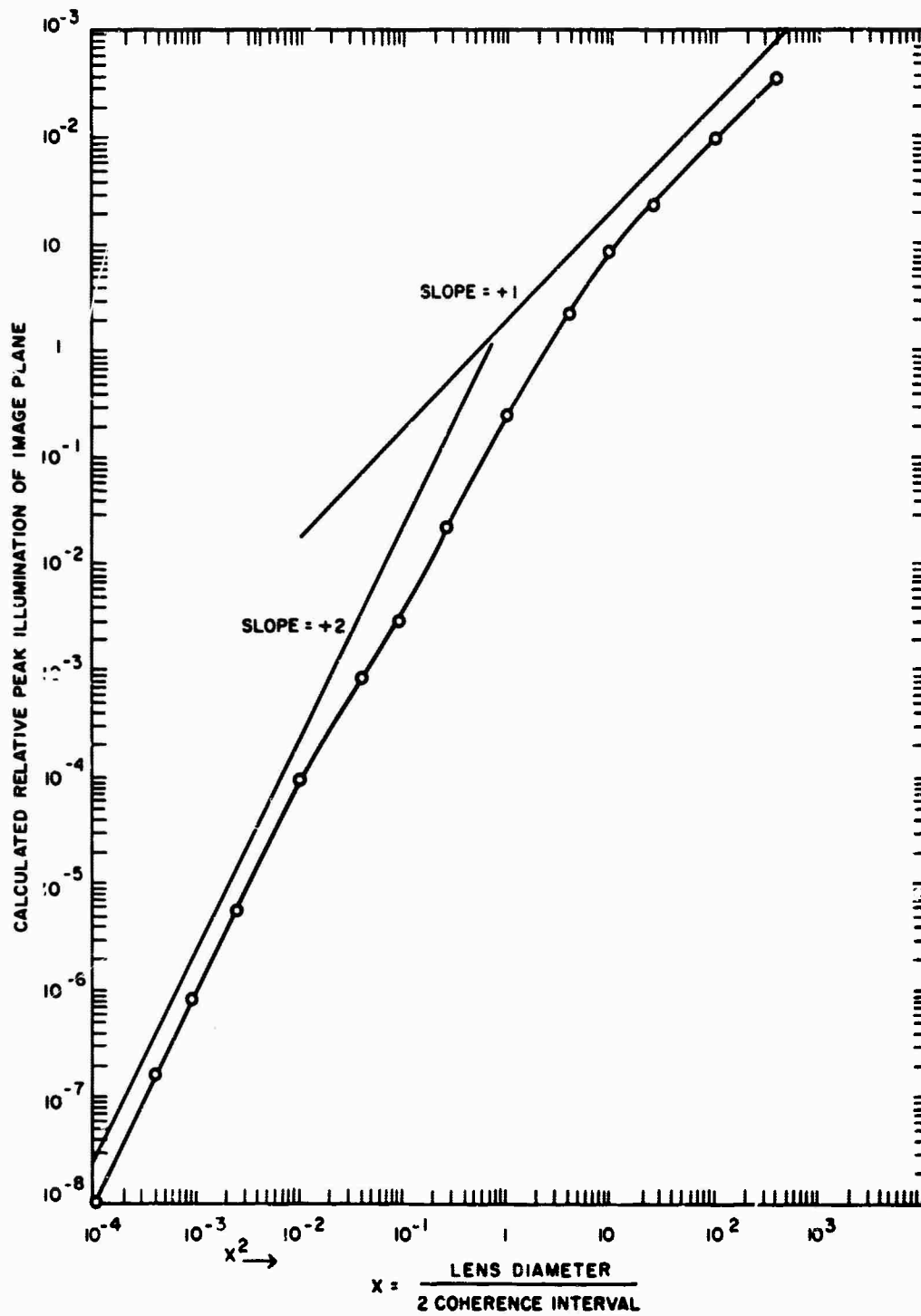
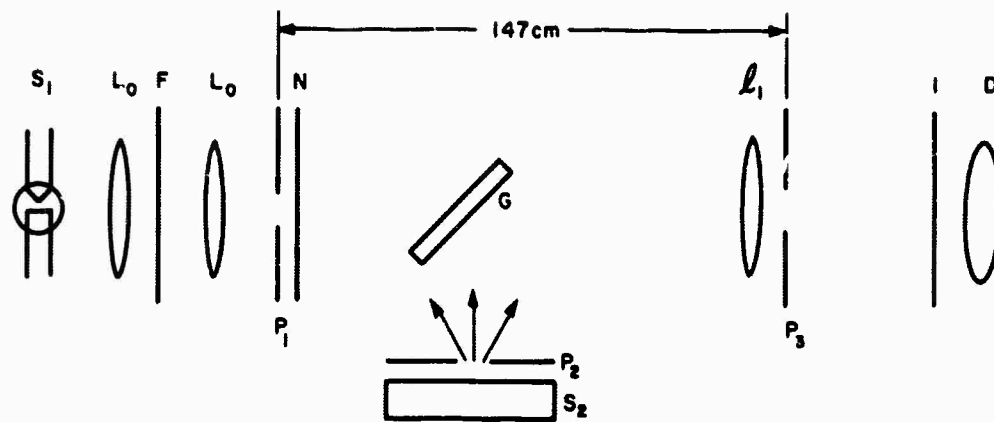


Figure 13. Variation of the Image Illumination from a Partially Coherent Field with Lens Aperture

For coherence intervals that are large compared to the lens diameter the central intensity goes as A^2 and at the other extreme as A . There is an essentially smooth transition between them. The difference in coherence interval between sky illumination and the illumination from a small object will mean that the transition region will occur at different values of the instrument aperture. If we concentrate for a moment on the region where both curves show linear increase with aperture, their separation on the energy scale for a fixed aperture value will be determined by their brightness. In this region both sources would be imaged and image brightness would, at best, equal source brightness. Thus, we can place a new interpretation on an old astronomical rule of thumb: increasing aperture aids discrimination. We are not really increasing the contrast between sky and star but merely recovering the inherent brightness difference that is available. The illumination from a near and a distant source will be different at the telescope aperture but the image brightness of each will be equal to the object brightness.

There are a variety of things that will modify this simple concept in practice. The sky illumination is from a distributed source so that no single plane is really an image plane. Also, the type of detector used will influence the result. Certainly, if the eye is used, then at some point the diffraction disc will become unresolvable and the effect of magnification will have to be included. These points will be further considered in a later section.

At the same time that the analysis was performed the problem was simulated on an optical bench. The experimental arrangement is shown in Figure 14. The sky background was simulated by a diffuse planar source and was folded onto the system axis by a beam splitter. Although this is a departure from the actual conditions, it corresponds more closely to the model used. The small source was a mercury arc image. Both sources were filtered so as to have approximately the same spectral composition. The image intensity was monitored with a 1P21 photomultiplier, with Panatomic-X film, and visually. The only visual measurement made was the value of the aperture when the small source was first noted and this was done with a clear image plane. The photomultiplier measurements were made through a 10μ hole at the center of the pattern. Figure 15 shows the value of the energy measured in this area as a function of aperture for the coherent and incoherent sources. The plot shown is log energy density vs log aperture. The slopes are 1.8 for the coherent source and 1.0 for the incoherent source. The discrepancy in the coherent energy can be accounted for by the fact that the fixed 10μ aperture measured a different fraction of the central diffraction disc at each aperture. Due to the range of aperture size necessary, no single source could be followed from its coherent to incoherent range. However, the analysis indicates that the slope of the coherent curve shown should begin to decrease at about 100 mm^2 of aperture. The experimental result seems to indicate that the restriction in the analytical approximation of the coherent case was too severe. The limit of visual perception, averaged over many attempts, was 144 mm^2 , which agrees fairly well. Controlled photographic exposures made over the region of the threshold indicated a similar value. Absolute photometric measurements of each field were made at several positions of the beam and in the focal plane, and the threshold of detection thus determined agreed well with the published curves of Knoll, Tousey, and Hulbert.³



- | | |
|-------|---|
| S_1 | 100 Watt mercury arc lamp (coherent point source) |
| S_2 | Aristo FGG-54 lamp (incoherent background) |
| L_0 | 32 mm f/1 objective lenses |
| F | 5461 Å interference filter |
| P_1 | 25 μ diameter pinhole |
| N | 4.6 neutral density filter |
| G | 6 cm diameter plate glass reflector |
| P_2 | 30 mm diameter aperture |
| l_1 | 52 cm f/1, 76 mm diameter imaging lens |
| P_3 | 23 mm diameter iris lens stop |
| I | Imaging plane |
| D | Detector |

Figure 14. Optical System with an Incoherent and Coherent Source Used for Determining Point Source Visibility

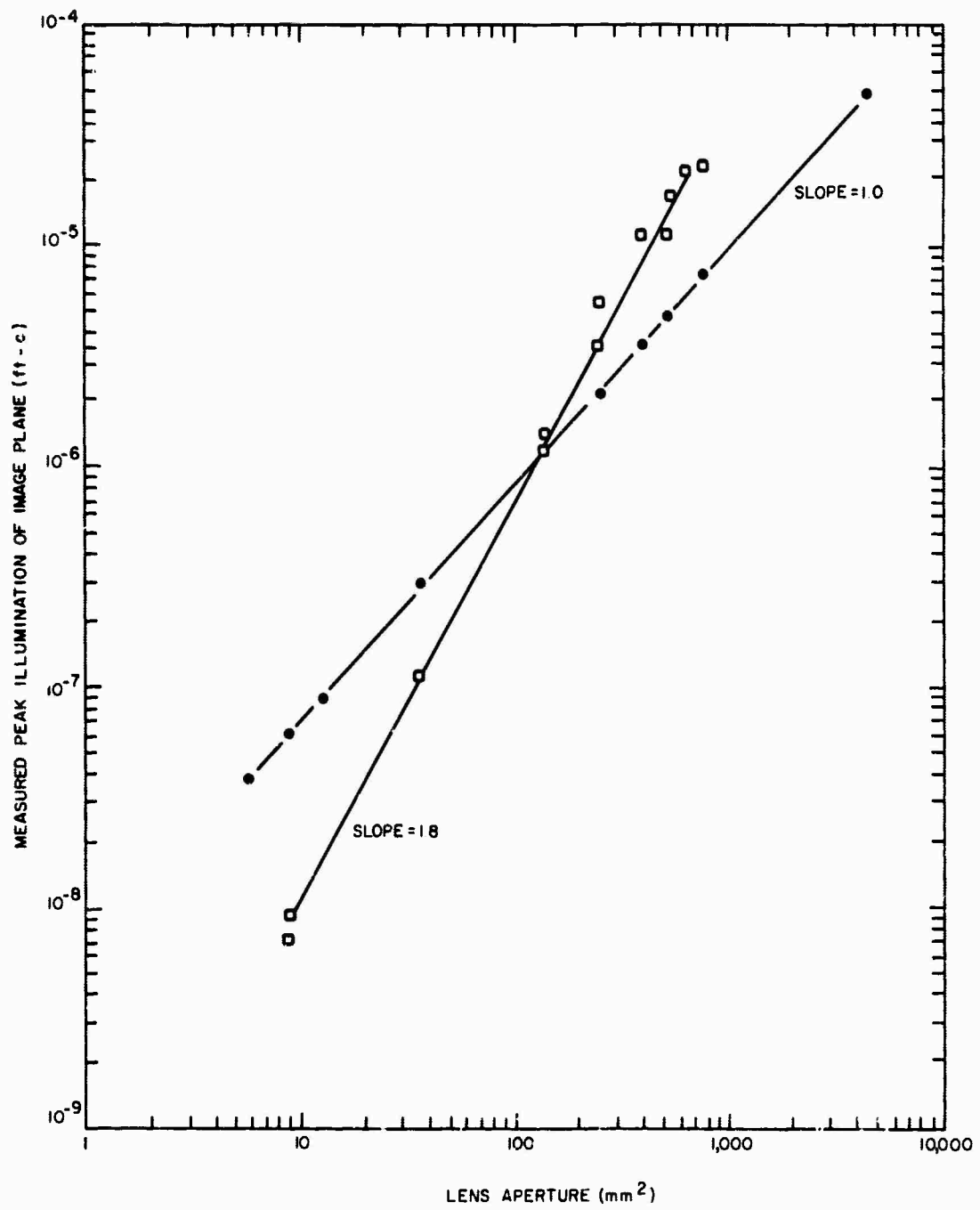


Figure 15. Variation of the Image Illumination from Coherent and Incoherent Sources with Lens Aperture

APODIZED LENS SYSTEMS WITH PARTIALLY COHERENT FIELDS

The experimental basis for this approach was provided by B. J. Thompson,⁴ who showed that if an array of apertures is incoherently illuminated, the increase in intensity of the diffraction pattern is proportional to the number of apertures in the array. It is known from the theory of diffraction gratings for a coherently illuminated array that the diffraction pattern intensity increases with the square of the number of apertures. The physical reasoning behind this approach is that a partially coherent field will show an energy variation somewhere between N^2 and N as the number of apertures is increased. Again, we wish to take advantage of the widely different coherence interval generated by each source. The solution to the general problem has been formally given by Thompson.⁴ However, the analytic form involves weighted sums over pairs of aperture points and is, in general, intractable. Another way of viewing this method is from the point of view of spatial filtering: we are attempting to maximize the signal-to-noise ratio in a system that is linear in the mutual coherence function. For the background, with its almost negligible coherence interval, the optical system will be, to a good approximation, linear in intensity. This means that the transfer function of the optical system must be an autocorrelation. We are trying to maximize the contrast subject to this constraint.

To further understand the properties of arrays in this connection, a series of experiments were performed. In the first experiment two sources with different coherence intervals were used. Each was made to illuminate first one and then a pair of apertures in front of the lens. The energy density at the center of the pattern was measured for all four cases. The spacing of the apertures was 2.0 mm and the coherence intervals of sources were 30.0 and 4.0 mm, corresponding to a degree of coherence between the apertures of 0.98 and 0.28, respectively. The change in energy was about 3 times greater for the first case and was close to 2 times greater for the second. The exact values deviate from the theoretical values because the energy must be collected over a finite area, which involves averaging over some portion of the distribution. The important observation is that the gain is between N and N^2 times the single aperture and is dependent on the coherence interval. The second experiment consisted of adjusting the experiment conditions with the background and a small source just invisible with a clear aperture and then placing several types of arrays over the aperture to determine if the threshold could be lowered. These experiments all yielded a negative result. We then began to analyze the array system in general to attempt to predict an optimum configuration for the types of fields we were using experimentally. It was obvious that whatever the particular geometry, it would be best to attempt to allow the number of apertures to increase indefinitely. There are some problems in how to take limit $N \rightarrow \infty$ in the proper way. If one continues to add finite-sized apertures, then ultimately one must have an infinite lens aperture, a decidedly nonphysical result. A more physical method is to place the first pair of apertures at the extremities of a fixed-diameter lens and then to fill the intervening area. To take the limit subject to a finite area, both the aperture area and the aperture separation must vanish. It is easy to see that the boundary of this operation is a clear aperture. One can also understand how this limit is reached by a physical argument. In the limit $N \rightarrow \infty$ the spatial frequency is also increasing without limit. This means that in the image plane the side bands are moving toward the edge of the field of view until only the central order is left. Therefore, the spatial filtering mode has the clear aperture as an upper boundary and ultimately the ratio of source brightnesses.

The use of a telescope in visual discrimination has been extensively investigated. We reviewed the established techniques to determine if a spatially filtered presentation in the image would improve any of these, but we do not find that any significant advantage can be obtained this way. In the following section we will briefly review some of general features of this subject.

CONVENTIONAL DETECTION TECHNIQUES

The general problem of detection of small, luminous objects against a bright sky background is a complex one, the solution of which involves the zenith angle of the object, its height, its azimuth from the sun, the condition of the atmosphere, the nature of the detector and detecting equipment, and the spectral range being used. Fortunately, however, most of these factors are fairly well understood and have been measured and analyzed in the literature of photometry and astronomy. Though many of the available derivations were made for the night sky, a carryover to the day sky can usually be made. The close connection between astronomical objects and the objects of interest in this study can be seen from the fact that the latter range from an angular subtend of 4×10^{-6} rad (0.8 sec) to 10^{-4} rad (20.5 sec). This places them in the size range of the planets whose angular size is given in Table I.

TABLE I
ANGULAR SIZE OF SELECTED PLANETS

| Planet | Angular Size (in seconds of arc) |
|---------|-------------------------------------|
| Mercury | 5.0 - 13.0 |
| Venus | 10.0 - 64.0 |
| Mars | 3.5 - 25.1 |
| Jupiter | 32.0 - 47.0 |
| Saturn | 14.0 - 20.0 |

The objects of interest produce an irradiation on the earth's surface of 10^{-12} to 10^{-10} W/cm². Assuming them to be black-body radiators, their peak luminous efficiency cannot exceed 0.14 ligat Watt/Watt. This would occur at 6,600°K and would correspond to 96 lu/W. Translated into lumens, therefore, the objects of interest may provide, at the earth's surface, an illumination of up to about 10^{-10} to 10^{-8} lu/cm², corresponding to an apparent visual magnitude (m) of m 0.8 to m -4.8. As shown in Table II, this again would place the objects in the range of planetary and stellar objects. If the calculations are valid, however, on reasonably so, it should be pointed out that the objects would appear as rather bright stars or planets when viewed at night with the naked eye and that any difficulty of detection would not be on account of their faintness, but only because of lack of contrast between them and the surrounding daylight sky.

TABLE II

APPARENT VISUAL MAGNITUDE OF SELECTED PLANETS

| Planet | Magnitude |
|---------|------------------------------------|
| Venus | -3.3 to -4.3 |
| Mars | +1.5 (at mean conjunction) to -2.9 |
| Jupiter | -2.4 (at mean opposition) |
| Saturn | +0.8 (at mean opposition) |

The sky background can be characterized either in the familiar units of luminance ($\text{lu}/\text{cm}^2 \text{sr}$ or related units) or in terms of magnitude per unit solid angle. The latter concept is frequently used by astronomers, particularly if the integration time of the detector is long in comparison with the fluctuations due to "seeing" and scintillation. The relationship between the two expressions is given by

$$m/\text{square second} = 2.37 - 2.5 \log B \text{ lu}/\text{cm}^2 \text{sr}.$$

For a clear-zenith sky, a typical low value of day-sky luminance is $0.2 \text{ lu}/\text{cm}^2 \text{sr}$. Using the above formula, we see that this corresponds to about $m 4/\text{sq deg}$, a value to be used in later calculations. Other day-sky luminance values for many regions of the sky, times of day, and positions of the sun have been measured extensively, for example by Barr.⁵

At least one aspect of the sky background problem has not been considered in the present survey: the relationship between the detectability of the object and its position in the atmosphere if the latter is considered as a three-dimensional scattering medium. In the case of astronomical objects, the atmosphere is clearly between the object and the observer. For the objects of interest in this survey, this may not be true, and certain corrections may have to be applied to the conclusions based on astronomical considerations.

PHOTOMETRY

If one ignores the specific detector type and considers only the lens system, one can see that a few simple expressions determine the photometry. First, if we neglect losses in the glass, the brightness of any image will equal the brightness of the object. Second, the illumination or energy per unit area of image, which is really of interest, is equal to the product of the brightness and the solid angle subtended by the exit pupil at the image. The use of these relations becomes modified by several things, among which are the type of detector and the atmospheric conditions.

The following survey is based on a search of the open literature. For convenience, it will be grouped according to the detectors used, i.e., the eye, photographic film, and photoelectric detectors. An attempt will be made throughout to point out not only the theoretical but also the practical aspects of the problem.

DETECTION

Photoelectric

Photoelectric detection of a small source in a background is a particular type of electrical noise problem. Since the background flux has shot noise statistics, one basically requires a signal level at least equal to the square root of the background level. Beyond this there are considerations of detector noise, spectral response, sensitivity, and bandwidth, which are discussed at some length by Whitford,⁶ Baum,^{7,8} and McGee.⁹

Photographic

In photographic detection, a single lens or mirror would normally be used. Here the detectability of the object would depend not only on the object, the sky luminance, the lens, and atmospheric factors, but also on the photographic emulsion and its development. According to Hynek,¹⁰ a combination of atmospheric effects and scattering within the emulsion will prevent the recording of a point source as a point but will record it as a small disc of the order of 50μ in diameter for telescopes over a large range of focal lengths. Within that range, the diameter of the disc is more or less independent of focal length. Table III shows the angle subtended by the sky at the lens (this is, of course, equal to that subtended by the disc at the lens) for different focal length lenses.

TABLE III
SKY ANGLE SUBTENDED BY 50μ DISC¹⁰

| Focal Length (in) | Angle (sec) |
|----------------------|----------------|
| 3 | 130.8 |
| 12 | 33.0 |
| 50 | 7.9 |
| 100 | 3.9 |
| 180 | 2.2 |
| 300 | 1.3 |

One can see from the table that a faint star will be more readily detected by a long-focal-length lens since, in this case, a smaller section of the sky competes with the star radiation within the 50μ disc.¹⁰ Whitford⁶ has shown how the same considerations can be treated quantitatively. Following Whitford, we can derive that

$$\log L_{\text{star}} = 2 \log D - 0.4 m - 8.97 \quad , \quad (9)$$

where L_{star} = lumens from the star accepted by the lens, D = the diameter of the telescope lens, and m = the visual magnitude of the star.

Similarly, for the clear-zenith day sky referred to previously,

$$\log L_{\text{sky}} = 2 \log D + 2 \log d/f - 0.5 \quad , \quad (10)$$

where L_{sky} = lumens from the sky section subtended and accepted by the lens, D = the diameter of the telescope lens, d = the diameter of the star image disc (including the effect of emulsion turbidity), and f = the focal length of the telescope. When the lumens from the star falling within the disc with diameter d are equal to the lumens arriving in the same area from the sky, we can equate the above equations and solve for the threshold magnitude, obtaining

$$m = -22.3 - 5 \log d/f \quad .$$

We note here that D has dropped out, that is, that the limiting detectable magnitude does not depend on the diameter of the lens.

Given the focal length of the telescope, we are now in a position to calculate the limiting visual magnitude by looking up the corresponding d/f value in the last column of Table III and substituting this in the equation for m .

For a 12-in. focal length lens, for instance, we obtain

$$m = -22.3 - 5 \log 1.6 \times 10^{-4} = -3.3 \quad . \quad (11)$$

In line with this, Hynek¹⁰ has reported on the successful photographic recording of several stars such as Capella and Polaris during the day. In the same paper he also briefly discussed the advantages of polarizing filters and the advantages and disadvantages of infrared emulsions compared with high contrast commercial panchromatic plates used in conjunction with red or blue filters.

Since, in the above calculations, there has been no assumption of a point-source image, the results can evidently be applied to sky objects other than stars, if an estimate can be made of the angular subtend (d/f) of their image.

It should be pointed out that Baum^{7, 8} has given an interesting theoretical treatment of photographic recording of astronomical objects in terms of the quantum efficiency of emulsions.

Visual¹¹⁻¹⁶

Naked-eye Observations — Although certain stars and planets can be seen at twilight,^{17,18} none can be seen without optical aid when the sun is at an altitude of more than about 15 deg above the horizon.¹⁹ In spite of occasional references in the literature²⁰ to the effect that stars can be seen during the day when viewed from the bottom of a deep shaft, Hynek¹⁰ and Smith²¹ showed experimentally (by viewing the sky through a long shaft) that the belief was without any foundation. Weaver¹⁹ calculated on the basis of laboratory experiments involving small, bright discs viewed against an illuminated background that, for a clear-zenith day sky, the star would have to be brighter than $m-2.1$ to be seen with the naked eye. The brightest star, Sirius ($m-1.6$), thus narrowly misses being detectable. Siedentopf²² had quite independently come to an essentially identical conclusion, though he suggested using a safety factor of 10. This would correspond to subtracting 2.5 from the calculated threshold magnitude.

One planet, Venus, can, however, be seen with the naked eye when the atmosphere is very clear, provided that the observer knows exactly where to look.^{17, 21} The latter provision arises from the fact that the light-adapted eye attains its full sensitivity only in the central fovea. Since Venus (see Table II) has a magnitude range of -4.3 to $m -3.3$, its visibility might be predicted from the data given in the paragraph above.

The Eye Aided by a Telescope — Tousey and Hulbert,²³ at Washington, D. C., detected six stars ranging from Sirius ($m -1.6$) to Spica ($m +1.2$) on a very clear day, using a telescope with high (20X) magnification. In their paper they point out the importance of using the highest possible magnification, M , that will still allow the object to be detected to be seen as a point, that is, that will still allow it to fall on one cone in the retina. This is because up to that magnification, for a given diameter objective, the background visual brightness will be inversely proportional to M^2 , while the brightness of the point image will be independent of M . The angle subtended by one cone is approximately 48 sec. If, because of atmospheric conditions, diffraction effects, or the apparent size of the object, this angle is approached, no further gain in detectability will result from an increase in magnification since now the object, too, would appear as an extended source whose apparent brightness would be decreased quadratically with any further increase in M . Bowen,²⁴ using older visual threshold contrast data, came to essentially similar conclusions.

In addition to using the "right" telescope, one should, of course, also be aware of the possibility of aiding the observations by use of spectrally selective filters and of polarizing filters, which can frequently reduce the light from the sky.

SECTION V

CONCLUSIONS AND RECOMMENDATIONS

The feasibility of an electronic fringe detector has been firmly established. A fringe detector operating in conjunction with a Fizeau interferometer has been designed, constructed, operated, and tested in the laboratory. Methods for analyzing the detecting system output have been established to optimize the sensitivity of the fringe detector from the standpoint of noise and discrimination techniques. The atmospheric noise inputs that degrade the resolution capabilities of both telescopes and interferometers have been analyzed, and the appropriate atmospheric research required has been defined. The possible use of a Michelson stellar interferometer to analyze the characteristics of pie-shaped sources has been analyzed by both a theoretical computer study and an experimental study. The pie-shaped source proved to have characteristics that are not particularly compatible with a Michelson stellar interferometer. Nonconventional optical techniques were examined to determine whether any gain in contrast between small-source and diffuse backgrounds could be obtained. The analysis of spatial filtering techniques for contrast enhancement indicates that no significant advantage can be gained by their use since their performance is inferior to that of an unapodized lens. The unapodized lens was shown to approach the ratio of source brightnesses as a performance limit.

FRINGE DETECTOR

A Fizeau interferometer-fringe detector combination was constructed with variable-separation apertures that can be adjusted from 0.6 to 6 cm. Aperture height was maintained at 0.1 times the separation. These apertures were in front of a 200 in. focal length optical system, which was used to produce a fringe pattern by superimposing the partially coherent light entering the two apertures. The fringe pattern was reflected by a rotating reflector and focused onto a single slit immediately in front of a phototube. The rotating reflector, single slit, and phototube combine to transform the spatially varying intensity pattern of the fringe field into a time-varying voltage signal displayed on an oscilloscope face. The oscilloscope trace was photographed and analyzed to determine fringe contrast.

The performance capabilities of the fringe detector are shown in Figure 6, which plots the fringe contrast required for detection as a function of watts per centimeter squared incident on the fringe detector. This is a general curve for any source in that the source brightness, size, and source-to-interferometer distance can be combined and expressed as watts per centimeter squared incident on the fringe detector.

There are four ways in which the performance of the fringe detector can be significantly improved in terms of sensitivity. If a grating instead of a slit were used to demodulate the fringes, a factor of 5 to 10 could be gained in sensitivity. A more sophisticated phototube (cooled) could provide a factor of 20 improvement in sensitivity. If the design of the entrance aperture were optimized for the particular

application of interest, it could provide a factor of 5 improvement. A further gain in sensitivity could be obtained by using long slits and a cylindrical lens as discussed under "Fringe Detector Design." This system would be useful only if measurement of fringe contrast at a single aperture separation were required. Overall, an ultimate fringe detector could be as much as 500 to 1000 times as sensitive as this instrument.

The following considerations and problems are involved in designing and constructing the optimum instrument. The integrals involved in designing the optimum configuration for the variable-separation apertures could only be evaluated on a computer, if then. A single grating cannot be used with variable-separation apertures because the optical design required (zoom lens) is impractical over the range of aperture separations required. Either the grating must be changed or a number of fringe detectors operating in parallel must be used to measure fringe contrast at different aperture separations. To maximize phototube sensitivity, the phototube must be cooled; it must have an optical response matched to the source; and it must have a photoemissive surface whose area is as small as possible consistent with the area of the grating. A specially designed phototube such as the phototube with the grating behind the photoemissive surface as described in "Fringe Detector Design" may be required. If the interferometer is to operate under conditions where the brightness of the source is fluctuating, or if there is an ambient background illumination present, then additional channels will be required as discussed under "Sources of Outside Noise."

In addition to higher resolution, the interferometer has advantages over the single-mirror telescope in that it can electrically filter out part of the noise due to image motion and ambient background illumination. The telescope can probably equal or surpass the interferometer when the source intensity is fluctuating. The important atmospheric parameters to study to compare the interferometer to the telescope are image motion and reductions in the complex degree of coherence due to atmospheric turbulence as well as ambient sky illumination and atmospheric-induced image motion.

PIE-SHAPED SOURCES

From the calculated values of fringe contrast, $|\gamma_{12}|$, we may conclude that the use of a Michelson stellar interferometer to study pie-shaped sources is more difficult than for simple circular sources. One reason is that $|\gamma_{12}|$ does not possess well-defined zeros, or maxima, which may be directly related to any one source characteristic such as radial or angular size. Also, even where a distinct and measurable pattern is apparent, which might be related to all the characteristic parameters of the source, the wide differences in intensity values or the extreme minuteness of detail and the lower overall illumination available (compared to a circular source) demand a very sensitive recording instrument.

DAYLIGHT DISCRIMINATION

The action of a lens system on the field due to an extended background and a small source was analyzed. The emphasis of the analysis was to consider such a system as linear in the mutual coherence function. The response for fields with arbitrary coherence for both apodized and unapodized systems was considered and it was shown that the apodized systems, which represent a spatial filtering system, have the unapodized case as a limit. A survey of the practical considerations reported in the literature for using a clear aperture instrument was made. Although the presentation of the filtered and clear aperture systems are different, it appears that no particular advantage in terms of contrast enhancement can be obtained by such systems.

REFERENCES

1. M. Born and E. Wolf, "Principles of Optics," 2nd ed. (New York, N.Y.: The Macmillan Company, 1964).
2. B.J. Thompson, R.A. Shore, and R.E. Whitney, "Diffraction by Apertures Illuminated with Partially Coherent Light," *J. Opt. Soc. Am.* 56, 733 (1966).
3. H.A. Knoll, R. Tousey, and E.O. Hulbert, "Visual Thresholds of Steady Point Sources of Light in Fields of Brightness from Dark to Daylight," *J. Opt. Soc. Am.* 36, 480 (1946).
4. B.J. Thompson, "Multiple Beam Interference," *J. Opt. Soc. Am.* 56, 1157 (1966).
5. N.L. Barr, "Brightness of the Atmosphere," Naval Medical Research Institute Research Report, Project No. NM 001 056.07.01, March 1953.
6. A.E. Whitford, "Limits of Sensitivity and Precision Attainable by Photoelectric Methods: Critical Summary and Comparison of Various Techniques," in Astronomical Photoelectric Photometry (Washington, D.C.: American Association for the Advancement of Science, 1953), 126.
7. W.A. Baum, "The Detection of Faint Images Against the Sky Background," *Trans. Int. Astr. Union* 9, 681 (1955).
8. W.A. Baum, "The Detection and Measurement of Faint Astronomical Sources," in Astronomical Techniques (Chicago, Illinois: The University of Chicago Press, 1962).
9. J.D. McGee, "Photo-Electric Aids in Astronomy," in Astronomical Optics and Related Subjects (New York, N.Y.: Interscience Publishers, Inc., 1956).
10. J.A. Hynek, "Photographing Stars in the Daytime," *Sky and Telescope* 10, 61 (1951).
11. H.R. Blackwell, "Contrast Thresholds of the Human Eye," *J. Opt. Soc. Am.* 36, 624 (1946).
12. P.W. Cobb and F.K. Moss, "The Four Variables of the Visual Threshold," *J. Franklin Inst.* 205, 831 (1928).
13. S.Q. Duntley et al., "Visibility," *Appl. Opt.* 3, 550 (1964).
14. S. Hecht, "Visual Thresholds of Steady Point Sources of Light in Fields of Brightness from Dark to Daylight," *J. Opt. Soc. Am.* 37, 59 (1947).

15. H. N. Russell, "The Minimum Radiation Visually Perceptible," *Astrophys. J.* 45, 60 (1917).
16. P. Fellgett, "Theoretical and Practical Explorations of the Use of Television Techniques in Astronomy," in *Astronomical Optics and Related Subjects* (New York, N. Y.: Interscience Publishers, Inc., 1956).
17. R. Tousey and M. J. Koomen, "The Visibility of Stars and Planets During Twilight," *J. Opt. Soc. Am.* 43, 177 (1953).
18. L. Wagenaar, "Visibility of Planets During Daylight," *J. Opt. Soc. Am.* 56, 406 (1966).
19. H. F. Weaver, "The Visibility of Stars Without Optical Aids," *Pub. Astron. Soc. Pac.* 59, 232 (1947).
20. G. S. Monk, "Light, Principles and Experiments," 2nd ed. (Magnolia, Mass.: Peter Smith Publishers, 1963).
21. A. G. Smith, "Daylight Visibility of Stars from a Long Shaft," *J. Opt. Soc. Am.* 45, 482 (1955).
22. H. Siedentopf, "Light in the Troposphere," in *Photometric and Radiometric Measurements in the Troposphere with Applications to the Visibility of Aerial Targets and Stars in Daylight Sky*, translated from the German by the Geophysics Research Directorate and published by Air Force Cambridge Research Laboratories, ARDC, as AFCRC-TN-55-210, 1955.
23. R. Tousey and E. O. Hulburt, "The Visibility of Stars in the Daylight Sky," *J. Opt. Soc. Am.* 38, 886 (1948).
24. I. S. Bowen, "Limiting Visual Magnitude," *Pub. Astron. Soc. Pac.* 59, 253 (1947).

| DOCUMENT CONTROL DATA - R&D | | |
|---|--|--|
| <i>(Security classification of title, body of abstract and indexing annotation must be entered when the overall report is classified)</i> | | |
| 1. ORIGINATING ACTIVITY <i>(Corporate author)</i> Technical Operations, Incorporated Burlington, Mass. | | 2a. REPORT SECURITY CLASSIFICATION Unclassified |
| | | 2b. GROUP |
| 3. REPORT TITLE INVESTIGATION OF ELECTRONIC FRINGE DETECTOR FOR A STELLAR INTERFEROMETER | | |
| 4. DESCRIPTIVE NOTES <i>(Type of report and inclusive dates)</i> Final Scientific Report Period covered: 7 April 1965 - 7 February 1967 | | |
| 5. AUTHOR(S) <i>(Last name, first name, initial)</i> Boa' nan, John and Kellen, Paul | | |
| 6. REPORT DATE 7 February 1967 | 7a. TOTAL NO. OF PAGES 49 | 7b. NO. OF REFS 24 |
| 8a. CONTRACT OR GRANT NO. AF 19(628)-5145 | 9a. ORIGINATOR'S REPORT NUMBER(S) TO-B 67-9 Final Report | |
| b. PROJECT AND TASK NO. 8663 | 9b. OTHER REPORT NO(S) <i>(Any other numbers that may be assigned this report)</i> AFCRL-67-0117 | |
| c. DOD ELEMENT 6250301R | | |
| d. DOD SUBELEMENT N/A | | |
| 10. AVAILABILITY/LIMITATION NOTICES Distribution of this document 's unlimited | | |
| 11. SUPPLEMENTARY NOTES Prepared for Hq. AFCRL, OAR (CRO) United States Air Force L. G. Hanscom Field, Bedford, Mass. | | 12. SPONSORING MILITARY ACTIVITY Advanced Research Projects Agency |
| 13. ABSTRACT <p>A fringe detector was constructed to detect fringes from a Michelson stellar interferometer and to relate these measurements to the characteristics of the source of illumination. A rotating reflector, a single slit, and a phototube were combined to transform the spatially-varying intensity pattern of the fringe field into a time-varying voltage signal displayed on an oscilloscope face. The oscilloscope trace was photographed and analyzed to determine fringe contrast.</p> <p>The maximum sensitivity of the detector was determined to be equivalent to a source providing 10^{-10} W/cm² at a fringe contrast of 1 and a signal-to-noise ratio of 1. Modifications can provide a factor of 500 to 1000 improvement in detector sensitivity. The interferometer was determined to have potentially better resolution than a single-mirror telescope because it can electrically filter the effects of ambient background illumination and turbulence. The use of an interferometer to measure the angular size of a pie-shaped source was studied and found to be not particularly suited to this purpose.</p> <p>The action of apodized and unapodized lens systems on the field due to an extended background and a small source was analyzed. The emphasis of the analysis was to consider such a system as linear in the mutual coherence function. The results indicate that no particular advantage in terms of contrast enhancement can be obtained by apodizing.</p> | | |

| 14. KEY WORDS | LINK A | | LINK B | | LINK C | |
|--|--------|----|--------|----|--------|----|
| | ROLE | WT | ROLE | WT | ROLE | WT |
| Electronic fringe detector Michelson Stellar interferometer Coherence Daylight discrimination | | | | | | |

INSTRUCTIONS

1. **ORIGINATING ACTIVITY:** Enter the name and address of the contractor, subcontractor, grantee, Department of Defense activity or other organization (*corporate author*) issuing the report.

2a. **REPORT SECURITY CLASSIFICATION:** Enter the overall security classification of the report. Indicate whether "Restricted Data" is included. Marking is to be in accordance with appropriate security regulations.

2b. **GROUP:** Automatic downgrading is specified in DoD Directive 5200.10 and Armed Forces Industrial Manual. Enter the group number. Also, when applicable, show that optional markings have been used for Group 3 and Group 4 as authorized.

3. **REPORT TITLE:** Enter the complete report title in all capital letters. Titles in all cases should be unclassified. If a meaningful title cannot be selected without classification, show title classification in all capitals in parentheses immediately following the title.

4. **DESCRIPTIVE NOTES:** If appropriate, enter the type of report, e.g., interim, progress, summary, annual, or final. Give the inclusive dates when a specific reporting period is covered.

5. **AUTHOR(S):** Enter the name(s) of author(s) as shown on or in this report. Enter last name, first name, middle initial. If military, show rank and branch of service. The name of the principal author is an absolute minimum requirement.

6. **REPORT DATE:** Enter the date of the report as day, month, year, or month, year. If more than one date appears on the report, use date of publication.

7a. **TOTAL NUMBER OF PAGES:** The total page count should follow normal pagination procedures, i.e., enter the number of pages containing information.

7b. **NUMBER OF REFERENCES:** Enter the total number of references cited in the report.

8a. **CONTRACT OR GRANT NUMBER:** If appropriate, enter the applicable number of the contract or grant under which the report was written.

8b, 8c, & 8d. **PROJECT NUMBER:** Enter the appropriate military department identification, such as project number, subproject number, system number, task number, etc.

9a. **ORIGINATOR'S REPORT NUMBER(S):** Enter the official report number by which the document will be identified and controlled by the originating activity. This number must be unique to this report.

9b. **OTHER REPORT NUMBER(S):** If the report has been assigned any other report numbers (*either by the originator or by the sponsor*), also enter this number(s).

10. **AVAILABILITY/LIMITATION NOTICES:** Enter any limitations on further dissemination of the report, other than those imposed by security classification, using standard statements such as:

- (1) "Qualified requesters may obtain copies of this report from DDC."
- (2) "Foreign announcement and dissemination of this report by DDC is not authorized."
- (3) "U. S. Government agencies may obtain copies of this report directly from DDC. Other qualified DDC users shall request through _____."
- (4) "U. S. military agencies may obtain copies of this report directly from DDC. Other qualified users shall request through _____."
- (5) "All distribution of this report is controlled. Qualified DDC users shall request through _____."

If the report has been furnished to the Office of Technical Services, Department of Commerce, for sale to the public, indicate this fact and enter the price, if known.

11. **SUPPLEMENTARY NOTES:** Use for additional explanatory notes.

12. **SPONSORING MILITARY ACTIVITY:** Enter the name of the departmental project office or laboratory sponsoring (*paying for*) the research and development. Include address.

13. **ABSTRACT:** Enter an abstract giving a brief and factual summary of the document indicative of the report, even though it may also appear elsewhere in the body of the technical report. If additional space is required, a continuation sheet shall be attached.

It is highly desirable that the abstract of classified reports be unclassified. Each paragraph of the abstract shall end with an indication of the military security classification of the information in the paragraph, represented as (TS), (S), (C), or (U).

There is no limitation on the length of the abstract. However, the suggested length is from 150 to 225 words.

14. **KEY WORDS:** Key words are technically meaningful terms or short phrases that characterize a report and may be used as index entries for cataloging the report. Key words must be selected so that no security classification is required. Identifiers, such as equipment model designation, trade name, military project code name, geographic location, may be used as key words but will be followed by an indication of technical context. The assignment of links, rules, and weights is optional.